

1 Dynamics of Variable Dusk-Dawn Flow Associated with Magnetotail 2 Current Sheet Flapping

3
4 James H. Lane¹, Adrian Grocott¹, Nathan A. Case¹, Maria-Theresia Walach¹

5
6 ¹ Department of Physics, Lancaster University, Lancaster, UK

7
8 Correspondence to: James Lane (j.lane@lancaster.ac.uk)

9 10 11 Abstract

12 We present Cluster spacecraft observations from 12 October 2006 of convective plasma
13 flows in the Earth's magnetotail. Earthward flow bursts with a dawnward $v_{\perp y}$ component,
14 observed by Cluster 1 (C1), are inconsistent with the duskward flow that might be expected
15 at the pre-midnight location of the spacecraft. Previous observations have suggested that
16 the dusk-dawn sense of the flow can be governed by the Interplanetary Magnetic Field
17 (IMF) B_y conditions, with the related 'untwisting hypothesis' of magnetotail dynamics
18 commonly invoked to explain this dependence, in terms of a large-scale magnetospheric
19 asymmetry. In the current study, observations of the upstream solar wind conditions from
20 OMNI, magnetic field observations by Cluster, and ionospheric convection data using
21 SuperDARN, indicate a large-scale magnetospheric morphology consistent with positive IMF
22 B_y penetration into the magnetotail. At the pre-midnight location of Cluster, however, the
23 dawnward flow observed below the neutral sheet by C1 could only be explained by the
24 untwisting hypothesis in a negative IMF B_y scenario. The Cluster magnetic field data also
25 reveal a flapping of the magnetotail current sheet; a phenomenon known to influence dusk-
26 dawn flow. Results from the curlometer analysis technique suggest that the dusk-dawn
27 sense of the $\mathbf{J} \times \mathbf{B}$ force was consistent with localized kinks in the magnetic field and the
28 flapping associated with the transient perturbations to the dusk-dawn flow observed by C1.
29 We therefore suggest that the flapping overcame the dusk-dawn sense of the large-scale
30 convection which we would expect to have been net duskward in this case. We conclude
31 that invocation of the untwisting hypothesis may be inappropriate when interpreting

32 intervals of dynamic magnetotail behaviour such as during current sheet flapping,
33 particularly at locations where magnetotail flaring becomes dominant.

34

35 **1. Introduction**

36

37 Convective magnetotail plasma flows at Earth, driven by the closing of magnetic flux via
38 reconnection as part of the Dungey Cycle (Dungey, 1961) have been studied extensively for
39 many years (e.g. Angelopoulos et al. 1992, 1994; Sergeev et al., 1996; Petrukovich et al.,
40 2001; Cao et al., 2006; McPherron et al., 2011; Frühauff & Glassmeier, 2016). Arguably, the
41 most well studied of these is the Bursty Bulk Flow (BBF). Angelopoulos et al. (1994) defined
42 BBFs as being channels of earthward plasma flow continually above 100 km s^{-1} , exceeding
43 400 km s^{-1} at one point across some interval, usually across a timescale of a few minutes.
44 The flows are said to be the main transporter of mass, energy and flux in the magnetotail
45 (e.g. Angelopoulos et al., 1994; Nakamura et al., 2002; Grocott et al., 2004a; Kiehas et al.,
46 2018). Although their earthward nature is the key defining characteristic of BBFs, they will
47 invariably exhibit a dusk-dawn component in their bulk flow as well (e.g. Angelopoulos et
48 al., 1994; Petrukovich et al., 2001; Grocott et al., 2004b). Understanding the drivers of dusk-
49 dawn asymmetries in magnetospheric dynamics is an important element of geospace
50 research (e.g. Haaland et al., 2017).

51

52 Magnetotail flows are generally expected to be symmetric about midnight (e.g. Kissinger et
53 al., 2012). A key factor that has been observed to influence the dusk-dawn direction of the
54 magnetotail flow, however, is the B_y component of the Interplanetary Magnetic Field (IMF).
55 It is well established that when the IMF reconnects with the dayside terrestrial magnetic
56 field, a non-zero IMF B_y component leads to asymmetric loading of open flux into the polar
57 cap (e.g. Khurana et al., 1996; Tenfjord et al., 2015; Grocott et al., 2017; Ohma et al., 2019).
58 This results in a twisting of the magnetotail whereby the closed field lines are rotated about
59 the midnight meridian, and a B_y component is superimposed onto the tail field as a
60 consequence of IMF B_y penetration (Cowley, 1981; Petrukovich, 2011; Tenfjord et al., 2015).
61 Subsequently, following nightside reconnection, the tail will untwist (Grocott et al., 2004c),
62 with the excitation of multiple convective flow bursts, each with an earthward and dusk-
63 dawn component, in the tail and nightside ionosphere (Grocott et al., 2007). In order to be

64 consistent with the tail ‘untwisting hypothesis’, any convective flows associated with an
65 individual tail field line should share the same dusk-dawn direction (e.g. see Figure 3 of
66 Grocott et al., 2005). The role of IMF B_y in the untwisting hypothesis has been examined
67 previously in a number of studies (e.g. Grocott et al, 2007; Pitkänen et al., 2013, 2015,
68 2017). These studies revealed that under prolonged positive IMF B_y conditions, the
69 earthward flows are expected to exhibit a dawnward component in the northern
70 hemisphere ($B_x > 0$) and a duskward component in the southern hemisphere ($B_x < 0$), with
71 the opposite correlation for negative IMF B_y conditions. This is especially true close to
72 midnight, where the penetration of IMF B_y is particularly noticeable. Further away from
73 midnight, however, effects such as magnetotail flaring (Fairfield, 1979) are expected to
74 product a dominant B_y component, which may suppress IMF B_y -effects on the dusk-dawn
75 asymmetry, resulting in the symmetric earthward convection of field lines (e.g. see Fig. 2 of
76 Pitkänen et al., 2019). Nevertheless, IMF B_y has been shown to govern the dusk-dawn
77 nature of these flows both during periods of steadier, slower convection (Pitkänen et al.,
78 2019), as well as during more transient, dynamic BBF-like intervals (Grocott et al., 2007) at
79 $|Y_{GSM}|$ values up to 7 R_E (Pitkänen et al., 2013). In the present study, we present Cluster
80 observations of dawnward and duskward directed flows that do not match this expected
81 dependence on IMF B_y , implying that the untwisting hypothesis is insufficient in this case. In
82 particular, we highlight the problematic nature of the observation of dawnward flow, in
83 relation to the pre-midnight location of Cluster. We instead suggest that the flows are being
84 driven by local perturbations due to dynamic behaviour of the tail that are associated with
85 flapping of the current sheet.

86

87 The current sheet, or ‘neutral’ sheet, lies in the equatorial plane at the center of the tail
88 plasma sheet and separates the earthward ($B_x > 0$) and tailward ($B_x < 0$) directed field (Ness,
89 1965). The current sheet is a highly dynamic region of the Earth’s magnetotail which can
90 undergo various types of net motion, such as tilting due to lobe magnetic pressures (Cowley
91 et al., 1981; Tenfjord et al., 2017) as well as flapping. Flapping of the current sheet can
92 generally be described as a sinusoidal-like variation in B_x of up to tens of nanoTesla, where
93 an observing spacecraft often measures repeated changes in the sign of B_x (e.g. Runov et al.,
94 2009), indicative of crossings of the current sheet, with characteristic times ranging from a
95 few seconds to (more commonly) several minutes (e.g. Runov et al., 2009; Wu et al., 2016;

96 Wei et al., 2019). Drivers of current sheet flapping have been widely investigated, with
97 possible causes ranging from external solar wind/IMF changes (Runov et al., 2009),
98 induction of hemispheric plasma asymmetries (Malova et al., 2007; Wei et al., 2015), fast
99 earthward flow (Nakamura et al., 2009) as well as periodical, unsteady magnetotail
100 reconnection (Wei et al., 2019). Studies such as Volwerk et al. (2008) and Kubyshkina et al.
101 (2014) have illustrated that flapping of the current sheet can be associated with variable
102 dusk-dawn flow, potentially overriding, or preventing any IMF B_y control of the flow.

103

104 In this paper we present Cluster spacecraft observations of an interval of dynamic
105 magnetotail behaviour on 12 October 2006, prior to which the B_y component of the
106 concurrent upstream IMF had been largely positive for several hours. Throughout this
107 interval, Cluster 1 observed oscillations in the magnetic field B_x component, which we
108 attribute to current sheet flapping, concurrent with a series of convective fast flows with
109 significant and variable dusk-dawn components. Observations from Cluster 2, 3 and 4
110 indicated that the spacecraft were at a pre-midnight location where magnetotail flaring was
111 dominating over IMF B_y control of the flows, resulting in the expectation of (symmetrical)
112 duskward return flows (Pitkänen et al., 2019). In the southern hemisphere, such duskward
113 flow was measured by Cluster 3, but not observed by Cluster 1, which instead measured
114 flows with significant dawnward components. These dawnward flows were therefore
115 inconsistent with any expectation that the flow was governed by flaring and, owing to
116 evidence of large-scale IMF $B_y > 0$ ionospheric convection pattern, could also not be
117 explained by the magnetotail untwisting hypothesis. We instead suggest that the current
118 sheet flapping was exciting the variable dusk-dawn flow, overriding the expected large-scale
119 duskward convection at the location of Cluster 1.

120

121 **2. Instrumentation and Data Sets**

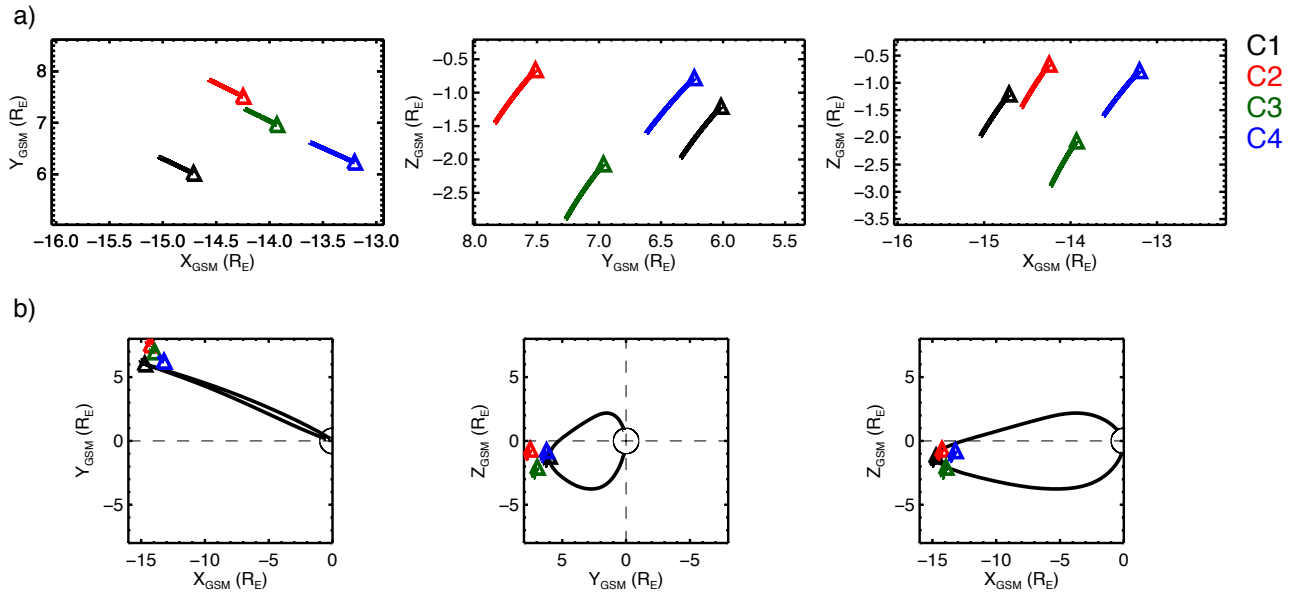
122 *2.1. Spacecraft Data*

123 The magnetospheric observations presented in this case study were made by the Cluster
124 multi-spacecraft (C1-C4) constellation (Escoubet et al., 2001). We make use of the fluxgate
125 magnetometer (FGM) onboard the Cluster spacecraft to obtain magnetic field
126 measurements (Balogh et al., 2001), and obtain our bulk ion velocity data from the Hot Ion
127 Analyser (HIA) on C1 and C3 calculated as on-board moments (Rème et al., 1997). The

128 magnetic field data presented are 5 vectors-per-second (0.2s res) which have been 1s
129 median-averaged, with the velocity data presented having spin resolution of just over 4s.
130 Where these datasets have been combined to produce parameters such as the plasma beta
131 and field-perpendicular velocities, we have resampled both the magnetic field and plasma
132 data to 5s resolution. All data are presented in geocentric solar magnetospheric (GSM)
133 coordinates unless stated otherwise.

134

135 The interval of study in this paper occurred between 00:00 – 00:55 UT on 12 October 2006.
136 At 00:00 UT the Cluster spacecraft were located in the near-Earth magnetotail plasma sheet,
137 in the pre-midnight sector. C1 was located at ($X = -14.7$, $Y = 6.0$, $Z = -1.2$) R_E , C2 at ($X =$
138 -14.2 , $Y = 7.5$, $Z = -0.7$) R_E , C3 at ($X = -13.9$, $Y = 7.0$, $Z = -2.1$) R_E , and C4 at ($X = -13.2$, $Y = 6.2$,
139 $Z = -0.8$) R_E . This is depicted in Fig. 1a by the colored triangles, along with the respective
140 spacecraft trajectories, from 00:00 – 00:55 UT, by the solid lines. Fig. 1b shows a zoomed-
141 out version of Fig. 1a, which illustrates the location of the spacecraft with respect to the
142 Earth. Fig. 1b also shows a traced modelled magnetic field line, achieved using the semi-
143 empirical TA15 model of the magnetosphere (Tsyganenko & Andreeva, 2015), which passes
144 through the location of C1 and connects to both the northern and southern hemispheres of
145 the Earth. We parameterised the TA15 model using mean-averaged solar wind dynamic
146 pressure (P_{dyn}), IMF B_y and IMF B_z data from the 1-hour interval prior to 00:28 UT (the start
147 of our specific interval of interest). These values were $P_{dyn} = 1.56$ nPa, IMF $B_y = +1.56$ nT and
148 IMF $B_z = -2.17$ nT. There was also a tailward dipole tilt of $\approx -12^\circ$. The model was also
149 parameterised with a solar wind coupling function index known as the ‘N index’, after
150 Newell et al. (2007). The N index varies between 0 (quiet) and 2 (very active), and in this
151 instance was ~ 0.4 .



152

153 **Figure 1:** a) The locations of the Cluster spacecraft in the X-Y, Y-Z, and X-Z GSM planes, from
 154 left to right, respectively, at 00:00 UT on 12 October 2006, marked by the triangles. The
 155 trajectories from 00:00 UT to 00:55 UT are marked by the solid lines. The spacecraft are
 156 color-coded according to the key on the right. b) As in a), with a zoomed-out view. The Earth
 157 is shown by the solid circle. A TA15 model magnetic field line passing through the location of
 158 C1 is shown as the solid black line.

159

160 The IMF measurements used in this study were provided by the OMNIweb database at 1-
 161 minute resolution, having been first propagated from L1 to the bow shock nose (King &
 162 Papitashvili, 2005).

163

164 2.2. SuperDARN Data

165 The ionospheric observations presented in section 3.3 were provided by the Super Dual
 166 Auroral Radar Network (SuperDARN), an international collaboration of 36 ground-based
 167 radars (Nishitani et al., 2019) that make line-of-sight Doppler measurements of the
 168 horizontal motion of the ionospheric plasma every few seconds (e.g. Chisham et al., 2007).
 169 Here, we use 2-min ionospheric convection maps created by fitting the line-of-sight $\mathbf{E} \times \mathbf{B}$
 170 velocity data to an eighth order expansion of the ionospheric electric potential in spherical
 171 harmonics using the technique of Ruohoniemi & Baker (1998), implemented in the Radar
 172 Software Toolkit (RST version 4.2, 2018). To accommodate intervals with limited data
 173 availability, the data are supplemented with values derived from a statistical model

174 parameterized by IMF conditions. This is a well-established technique that has been
175 thoroughly discussed by, e.g., Chisham et al. (2007). The convection maps we present
176 employ the commonly used model of Ruohoniemi & Greenwald (1996). As a check on the
177 sensitivity of the maps to the choice of model input, we also tested the fitting using the
178 alternative model of Thomas and Shepherd (2018) and found that this has little impact on
179 the maps and no impact on our conclusions.

180

181 As a further measure to ensure that the choice of model is not critical to our results, we
182 chose not to use the concurrent IMF vector to parameterise the background model. In this
183 case, because we are using the SuperDARN data to provide evidence in support of the
184 expected large-scale influence of IMF B_y , we deemed it inappropriate to include model data
185 already parametrised by IMF B_y . We instead specify a nominal southward IMF with zero B_y
186 component in our analysis, to ensure that a background model with no pre-existing IMF B_y
187 influence is used. Although this might result in the patterns we show being less accurate
188 overall, especially in regions of poor data coverage, it will ensure that any B_y -associated
189 asymmetry in the maps is driven by the radar data from our interval of study, and not the
190 background model. This is discussed further in section 4.1, below.

191

192 **3 Observations**

193

194 In this section we present observations of the IMF, magnetotail magnetic field and plasma
195 flow, and ionospheric convection from an interval on 12 October 2006.

196

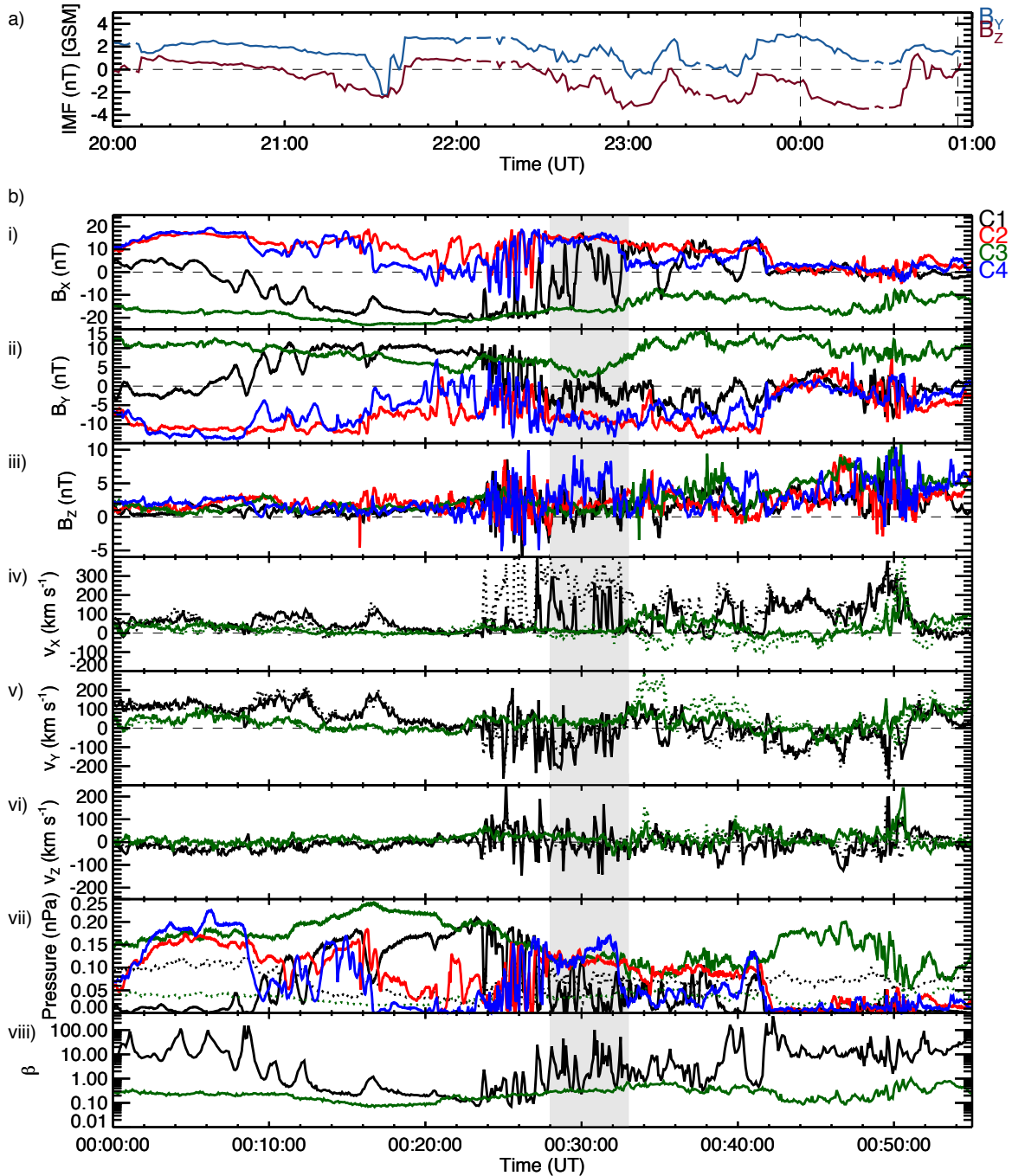
197 *3.1 IMF Observations*

198 Figure 2 presents an overview of the spacecraft data from an extended interval around our
199 period of specific interest for broader context. In Figure 2a, we show a time-series of the
200 IMF B_y and IMF B_z data from 20:00 UT on 11 October to 01:00 UT on 12 October 2006. These
201 data reveal that IMF B_y was generally positive for several hours prior to the fast flow
202 interval, with IMF B_z predominantly negative. There were three small intervals of negative
203 IMF B_y at \sim 21:35 UT, 23:00 UT and 23:40 UT and we discuss the possible ramifications of
204 these, and our treatment of them, in section 4.1.

205

206 3.2 Cluster Spacecraft Observations

207 In Figure 2b, we present the in-situ magnetic field and plasma measurements from the
 208 Cluster spacecraft across the interval 00:00 – 00:55 UT.
 209



210
 211 **Figure 2:** a) A plot of the IMF time series data for the IMF B_y (blue) and IMF B_z (red)
 212 components, from 20:00 UT on 11 October 2006 to 01:00 UT on 12 October 2006. The
 213 vertical dashed lines indicate the start (00:00 UT) and end (00:55 UT) of the interval of

214 Cluster data (below). b) The in-situ Cluster spacecraft measurements. Shown first is the local
 215 magnetic field data, i) B_x , ii) B_y and iii) B_z , followed by the bulk ion velocity data, iv) v_x , v) v_y ,
 216 and vi) v_z (dotted lines). The field-perpendicular component of the ion flow (indicative of
 217 the $\mathbf{E} \times \mathbf{B}$ convection) is shown in panels iv) to vi) by the solid lines. In panel vii) the magnetic
 218 $\left(\frac{B^2}{2\mu_0}\right)$ and thermal ion (nkT) pressures are shown by the solid and dotted lines respectively,
 219 and in panel viii) the ion plasma beta from C1 and C3 is shown. All data are labelled
 220 according to the color-coded key on the right-hand side. The time-interval between the gray
 221 shaded region marks our specific interval of interest (discussed in text).

222

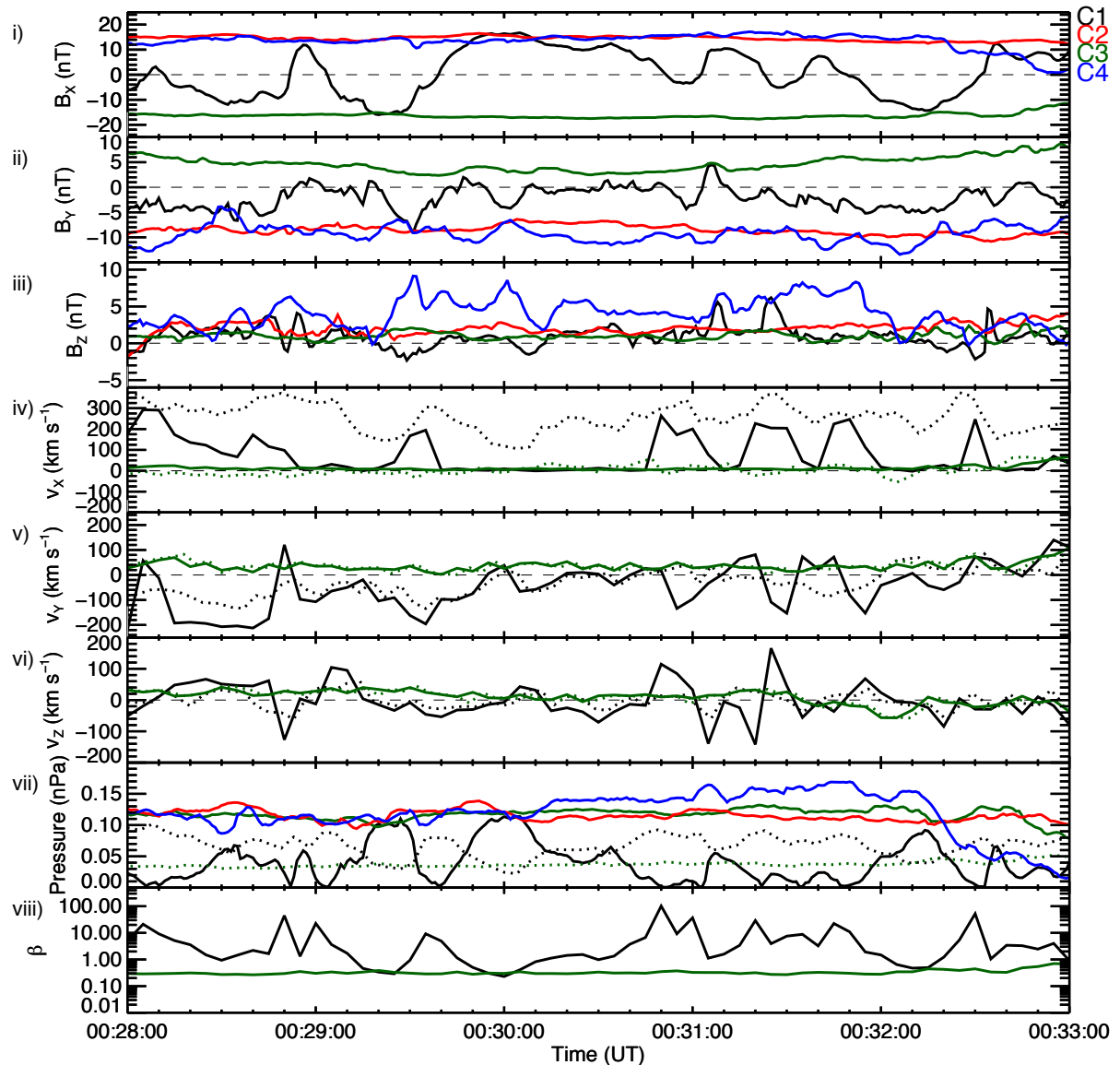
223

224 At $\sim 00:06$ UT, C1 crossed from the northern hemisphere into the southern hemisphere,
 225 illustrated by the sign change in B_x from positive to negative shown in Fig. 2b i). Coincident
 226 with this, the observed B_y , shown in Fig. 2b ii) turned from negative to positive, consistent
 227 with the expected B_y due to magnetotail flaring (see section 4.2) at this pre-midnight
 228 location (Fairfield, 1979). Fig. 2b iv) reveals that up until $\sim 00:24$ UT, the bulk earthward flow
 229 (v_x , dotted lines) and field-perpendicular flow ($v_{\perp x}$, solid lines) measured by both C1 and C3
 230 was generally low in magnitude ($< 100 \text{ km s}^{-1}$). The dusk-dawn (v_y) component of the flow,
 231 shown in Fig. 2b v), remained steadily duskward ($v_y > 0$) at C1 and duskward or close to zero
 232 at C3. The north-south (v_z) component of the flow in Fig. 2b vi), measured by C1 and C3 was
 233 effectively zero. During this period, the Cluster spacecraft that resided in the northern
 234 hemisphere (predominantly C2 and C4), observed $B_y < 0$, and the spacecraft which resided
 235 in the southern hemisphere (predominantly C1 and C3) observed $B_y > 0$, again consistent
 236 with magnetotail flaring. Occasionally a spacecraft encountered the current sheet ($B_x = 0$) at
 237 which point it observed $B_y = 0$. We comment on the significance of these magnetic field
 238 observations in section 4.2.

239

240 After $\sim 00:24$ UT, C1 began to observe a period of enhanced earthward flow
 241 ($v_x > 300 \text{ km s}^{-1}$) and variable dusk-dawn flow, concurrent with sudden variation in the local
 242 B_x component. Similarly, C2 and C4, but not C3, observed large magnitude ($> 20 \text{ nT}$) rapid
 243 variations in B_x , which appear to have an apparent timescale of around a minute and which
 244 we attribute to a flapping of the current sheet. As well as rapid variations in B_x , both the B_y

245 and B_z components of C1, C2 and C4 seemed highly variable. As perhaps to be expected,
246 these variations in the magnetic field were accompanied by significant variations in the
247 magnetic pressure of ~ 0.15 nPa, as shown by the solid lines in Fig. 2b vii).
248 Unlike the other spacecraft, C3 remained in the southern hemisphere throughout the entire
249 interval and did not observe the rapid fluctuations in B_x . Between 00:28 – 00:33 UT (the gray
250 shaded region), C1 began to repeatedly and rapidly cross the current sheet, as previously
251 experienced by C2 and C4, whilst continually observing enhanced earthward flow and
252 variable dusk-dawn convective flow ($v_{\perp y}$). Across the entire interval, the plasma beta, β ,
253 indicated in Fig. 2b viii), measured by C3 remained above ~ 0.1 , with C1's measured β
254 ranging from 0.1 to over 100. This is consistent with the fact that C1 was continually
255 crossing the current sheet at the center of the plasma sheet, where β is larger (Baumjohann
256 et al., 1989). It is this interval of current sheet crossing and variable flow observed by C1
257 that we focus on below and is presented in more detail in Figure 3.



258

259 **Figure 3:** As in Fig. 2b, but for the interval 00:28 – 00:33 UT on 12 October 2006.

260

261 Fig. 3 i) conveys the extent of the large-amplitude B_x variations observed by C1 between

262 00:28 and 00:33 UT. B_x was generally fluctuating between positive and negative values

263 throughout the five-minute interval, with a minimum at ~ -16 nT and maximum at ~ 17 nT.

264 The magnetic pressure at C1 shown by the solid black line in Fig. 3 vii) is consistent with the

265 idea that C1 was crossing the current sheet, as this generally reached minima at the center

266 of each current sheet crossing ($B_x \approx 0$). The B_y component (Fig. 3 ii) measured by C1 generally

267 remained negative and highly variable for the entire interval, with a number of large

268 negative enhancements and a few small positive excursions. It is particularly of note that

269 when C1 was below the neutral sheet, as implied by a negative B_x component, B_y was

270 almost always negative. As we discuss in section 4.2, this is inconsistent with what we would
 271 expect based on the location of the spacecraft and also inconsistent with any expectation
 272 that a positive IMF B_y should have penetrated into the tail. The B_z component (Fig. 3iii)
 273 generally remained positive with some small negative excursions.

274

275 Unlike C1, C2-4 measured generally steady B_x throughout this five-minute period. C2 and C4
 276 measured positive B_x , indicating that they were above the neutral sheet, and C3 measured
 277 negative B_x , indicating that it was below the neutral sheet. Similarly, B_y was steadily negative
 278 for C2 and C4 and steadily positive for C3. These observations are consistent with the larger-
 279 scale B_y at the spacecraft location being dominated by magnetotail flaring. Again, we note
 280 the inconsistency between the C1 and C3 observations of B_y ; when in the southern
 281 hemisphere C1 generally observed $B_y < 0$, whereas C3 observed $B_y > 0$. On a few separate
 282 occasions C1 did briefly observe $B_y > 0$ (e.g. at 00:31:05 UT) but at these times C1 was
 283 located above the neutral sheet ($B_x > 0$), while C2 and C4 observed $B_y < 0$ above the neutral
 284 sheet. These variations in B_y imply the observation of a ‘kink’ in the field at the location of
 285 C1, the ramifications of which are discussed further in section 4.2.

286

287 At times when B_x observed by C1 was negative, indicating that C1 was below the neutral
 288 sheet, C1 generally observed negative (dawnward) $v_{\perp y}$ (Fig. 3v) with a magnitude varying
 289 between 100 and 200 km s⁻¹. At times when B_x became positive, indicating that C1 was
 290 above the neutral sheet, C1 observed positive (duskward) $v_{\perp y}$ a majority of the time,
 291 although this flow barely reached 100 km s⁻¹. The negative enhancements in $v_{\perp y}$ were
 292 generally accompanied by negative enhancements in B_y . Across the interval, there was a
 293 near continual $v_x > 200$ km s⁻¹ flow (black dotted line in Fig. 3iv), peaking at almost 400 km
 294 s⁻¹, with concurrent peaks in the convective $v_{\perp x}$ component (solid black line) of at least
 295 200 km s⁻¹. The convective flow measured by C3, however, was generally very weak ($|v_{\perp}| <$
 296 50 km s⁻¹) throughout this period (solid green line in Fig 3iv). v_z (Fig. 3vi), as measured by
 297 both C1 and C3 remained low in magnitude (< 100 km s⁻¹) for the duration of the interval,
 298 with a few $v_{\perp z}$ excursions above 100 km s⁻¹ observed by C1. The most significant
 299 enhancements in $v_{\perp z}$ seen by C1 appeared to occur in conjunction with the rapid current
 300 sheet crossings between 00:30:50 and 00:32:00 UT. We discuss the implications of these

301 observations in the context of the upstream IMF conditions and large-scale magnetospheric
302 morphology in section 4.

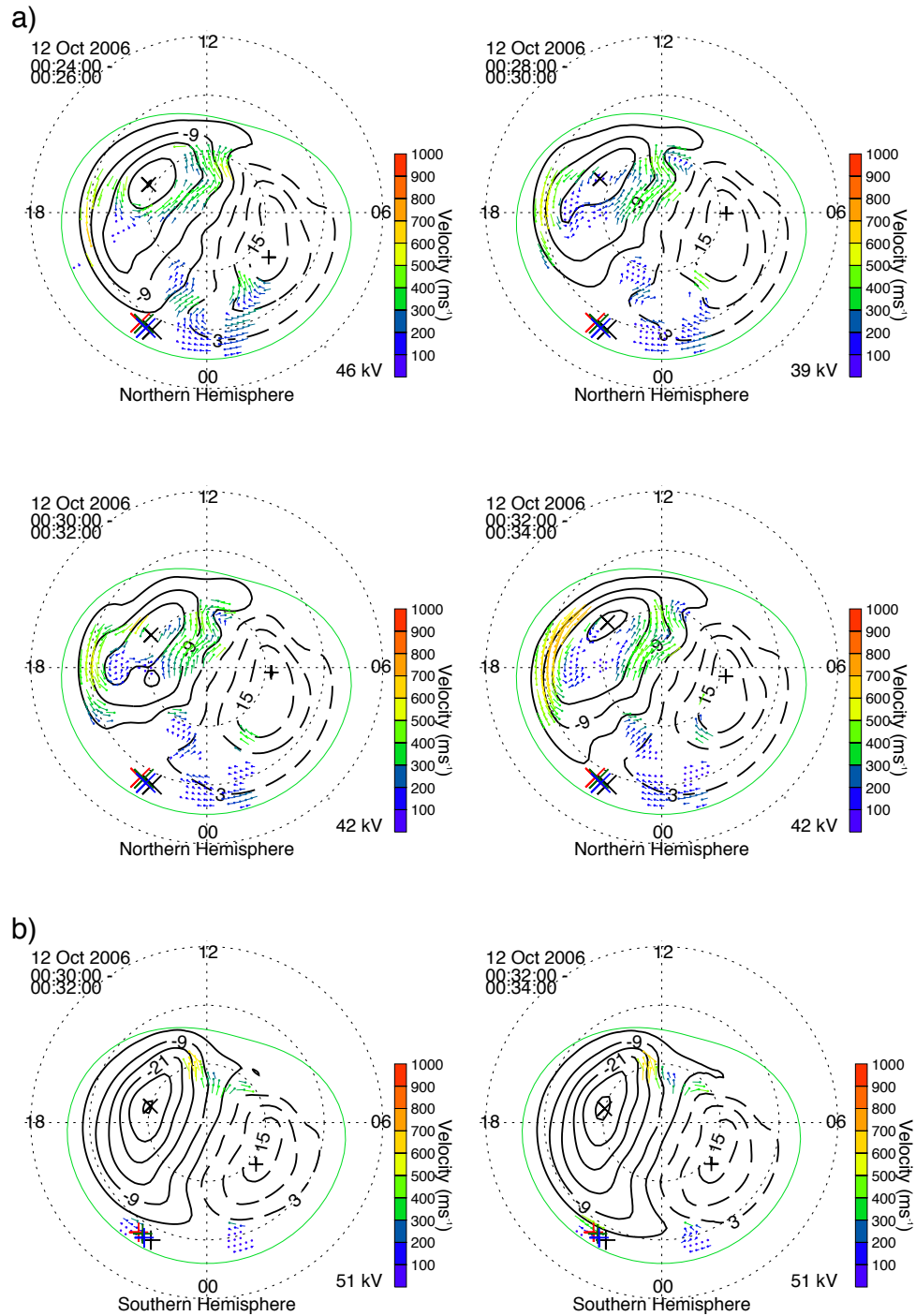
303

304

305 *3.3 Ionospheric Convection Observations*

306

307 To provide the large-scale context in which we can interpret the more localized
308 observations from the Cluster spacecraft we show ionospheric convection observations in
309 Figure 4. In Fig. 4a we present a series of four 2-minute integration SuperDARN maps of the
310 northern hemisphere ionospheric convection pattern, beginning at 00:24 UT, and ending at
311 00:34 UT, which encompasses our specific interval. In all maps, plasma is flowing anti-
312 sunward across the polar cap at high latitudes, also with a strong duskward sense, with the
313 direction of the convection reversing in the pre-midnight sector before returning sunward at
314 lower latitudes.



315

316

317

318

319

320

321

322

Figure 4: Maps of the ionospheric plasma convection derived from SuperDARN observations. Midnight is to the bottom of each map, noon to the top, dusk to the left and dawn to the right. The dashed black circles are spaced every 10° in magnetic latitude. The thicker solid and dashed black lines represent the plasma streamlines and are the contours of the electrostatic potential. Flow vectors are plotted at the locations of radar observations and these are color-coded based on the magnitude of their velocity. a) Four 2-minute northern hemisphere maps from 00:24 – 00:26, 00:28 – 00:30, 00:30 – 00:32 and 00:32 –

323 00:34 UT, respectively. b) Two 2-minute southern hemisphere maps from 00:30 – 00:32 and
324 00:32 – 00:34 UT, respectively. On each northern (southern) hemisphere map, the
325 footpoints of the Cluster spacecraft constellation are shown by the X's (+'s), mapped using
326 the TA15 model.

327

328

329 Owing to the coupled nature of the magnetosphere-ionosphere system, the observed
330 ionospheric convection pattern is indicative of the global-scale magnetospheric convection
331 (Cowley, 1981). In this case, the typical symmetrical twin-cell convection pattern has been
332 rotated clockwise, with the dawn cell extending across into the pre-midnight sector,
333 indicative of convection that has been driven under the influence of a positive IMF B_y
334 component (e.g. Reistad et al., 2016, 2018). On each northern hemisphere map, the
335 footpoints of the Cluster spacecraft constellation are indicated by the crosses (X), mapped
336 using the TA15 model with the same parameterisation described in section 2.

337

338 Fig. 4b shows two 2-minute integration SuperDARN maps of the southern hemisphere
339 ionospheric convection pattern, beginning at 00:30 UT, and ending at 00:34 UT. The
340 associated footpoints of the Cluster spacecraft are indicated by the plus signs (+). Although
341 the coverage of radar data is much less than in the northern hemisphere, there are data in
342 the pre- and post-midnight sectors which appears to be influencing the location of the flow
343 reversal region at the nightside end of the dusk cell. Opposite to the northern hemisphere
344 case, it is the dusk cell in the south which is extending towards, or just beyond, the midnight
345 meridian. This is also consistent with a large-scale positive IMF B_y influence, owing to the
346 expected north-south asymmetry of the influence of IMF B_y in the magnetosphere (e.g.
347 Pettigrew et al., 2010). The significance of these observations is further discussed in section
348 4.1.

349

350 **4. Analysis and Discussion**

351

352 We have presented observations of a dynamic interval of plasma flows and magnetic field in
353 the Earth's magnetotail. In this section we discuss our rationale for interpreting the flows
354 observed by C1 as being inconsistent with the large-scale convection expected based on the

355 spacecraft location and magnetotail untwisting considerations, and our alternative
356 interpretation of their relationship to current sheet flapping.

357

358 *4.1 Evidence for an inconsistency with large-scale magnetotail untwisting*

359 During the five-minute interval studied (00:28 – 00:33 UT) C1 measured a continually
360 fluctuating B_x component (Fig. 3i), indicative of multiple crossings of the tail current sheet.
361 C1 was the only spacecraft to measure this signature across the interval (although similar
362 signatures had been observed a few minutes earlier by C2 and C4). C1 also measured a
363 series of earthward convective magnetotail fast flows with varying dusk-dawn components.
364 The data in Fig. 3 i) and Fig. 3 v) illustrate that when B_x was positive (negative), a duskward
365 (dawnward) $v_{\perp y}$ was generally observed. The observed downward flow in the southern
366 hemisphere, in particular, is inconsistent with the expected symmetric duskward flow at the
367 pre-midnight location of C1 which was, however, observed by C3. This suggests that the
368 typical ‘symmetrical’ Dungey-cycle return flow (e.g. Kissinger et al., 2012) cannot provide an
369 explanation for the flow observations made by C1. We thus turn our attention to other
370 possible explanations which we explore in detail, below.

371

372 The data in Fig. 3 ii) show that C1 tended to observe a negative B_y component. According to
373 the magnetotail untwisting hypothesis (e.g. Pitkänen et al., 2015), these flow and magnetic
374 field observations are consistent with a negative IMF B_y penetration. The IMF data
375 presented in Fig. 2a, on the other hand, revealed that IMF B_y was generally positive for
376 several hours prior to the fast flow interval (00:28 – 00:33 UT). Based on the IMF data alone,
377 therefore, one might expect that a positive IMF B_y will have penetrated into the
378 magnetosphere and thus ought to have determined the “expected” dusk-dawn direction of
379 the flow. In that case, the flows observed here would have a dusk-dawn sense that is not
380 explained by current theoretical models of magnetotail untwisting, meaning they are not
381 IMF B_y -controlled (e.g. Grocott et al., 2007). There are a number of possible explanations for
382 this discrepancy and we address each one in turn.

383

384 The first possibility is that our conclusion regarding the expected sense of IMF B_y control is
385 incorrect. As discussed above, the flows observed by Cluster would be consistent with the
386 magnetotail untwisting hypothesis in the case that we had IMF $B_y < 0$ penetration. We

387 noted in section 3.1 that there were three small negative IMF B_y excursions prior to our
388 Cluster observations interval. Although the propagation of the IMF to the bow shock is
389 accounted for in the OMNI data, there is uncertainty regarding the time it takes for the IMF
390 B_y to 'propagate' into the magnetotail. Uncertainties in IMF B_y propagation times (e.g. Case
391 & Wild, 2012) have previously been cited as an explanation for observing an unexpected
392 asymmetry (e.g. Pitkänen et al., 2013). Studies such as Tenfjord et al. (2015, 2017) and Case
393 et al. (2018), for example, have suggested a reconfiguration time (to the prevailing IMF B_y
394 conditions) for nightside closed field lines of around 40 minutes. At ~00:28 UT (the
395 beginning of our specific interval of interest), the IMF B_y had been positive for around
396 50 minutes. Based on the Tenfjord timescale, this would thus imply that our interval was
397 wholly IMF $B_y > 0$ driven. Other studies, on the other hand, such as Browett et al. (2017),
398 have shown that longer timescales of a few hours may be important.

399

400 However, for such long timescales to play a role one would expect to have observed a
401 relatively persistent IMF B_y component during that time. The integrated IMF B_y over the
402 hours prior to our interval was certainly convincingly B_y -positive, and it seems highly unlikely
403 that a few minute-long fluctuations into the opposite IMF B_y polarity, 1 or 2 hours prior to
404 the flows we observed, could have a significant influence. We can thus be confident that
405 positive IMF B_y was governing the global magnetospheric dynamics in this case.

406

407 Despite this convincing argument that the IMF data alone imply a positive IMF B_y
408 penetration, we performed an additional analysis to further ensure that these negative
409 excursions did not lead to a change in the global nature of the magnetosphere-ionosphere
410 system. We inspected the concurrent northern hemisphere SuperDARN data (presented in
411 Fig. 4a) to provide evidence of the large-scale convection pattern. If the large-scale flow is
412 consistent with a positive IMF B_y component, then the magnetotail flows that we observed
413 must be deviating from this for some reason and cannot be related to IMF B_y control. The
414 SuperDARN data indeed confirm that the large-scale morphology of the system was
415 consistent with a positive IMF B_y component (e.g. Lockwood 1993; Grocott et al., 2017;
416 Reistad et al., 2018). This can be inferred from the general shape of the convection pattern,
417 whereby across multiple maps (00:24 – 00:34 UT) the pattern was rotated clockwise, with
418 the dawn cell having extended into the pre-midnight sector. That this is the expected

419 convection pattern for an IMF B_y -driven magnetosphere is also supported by the concurrent
420 low level of geomagnetic activity. The auroral AU and AL indices (not shown) confirm that
421 this interval is geomagnetically quiet (AU and |AL| both less than (or of the order of) 10 nT),
422 such that the nightside ionospheric convection asymmetry should be driven by IMF B_y rather
423 than conductivity-driven features such as the Harang reversal which might otherwise
424 complicate the auroral zone flows (e.g. Grocott et al., 2007; Grocott et al., 2008; Reistad et
425 al., 2018).

426

427 The validity of the convection observations is further supported by the coverage of nightside
428 data which were used to constrain the model convection pattern. The data used to create a
429 SuperDARN convection map are supplemented by data from a statistical model (in this case
430 Ruohoniemi & Greenwald, 1996) which is typically parameterised by the instantaneous IMF
431 conditions. In the case that there is a lack of real data coverage, a created SuperDARN map
432 will be strongly influenced by the model data, as opposed to real data, and thus would
433 reflect a prediction of convection based on the IMF conditions. The maps shown in Fig. 4a
434 illustrate that there were dozens of SuperDARN vectors in the midnight sector which were
435 fitted to create the global convection maps. To confirm that these data were sufficient, and
436 that the observed large-scale convection pattern was not being driven by model data, we
437 parameterised the model in our analysis with IMF $B_y = 0$. Despite this, a clear IMF B_y -
438 asymmetry exists, thus demonstrating that the observed large-scale IMF $B_y > 0$ global
439 convection patterns must be data-driven.

440

441 A second possible explanation for the discrepancy between the dusk-dawn direction of the
442 local and global-scale convection concerns the certainty with which we can determine the
443 location of the spacecraft with respect to the large-scale convection pattern. The untwisting
444 hypothesis, as considered by e.g. Pitkänen et al. (2013, 2017), relies on the assumption that
445 the convection cell to which the spacecraft is connected should be a factor of only
446 hemisphere and the sense of IMF B_y . In other words, as discussed above, for IMF $B_y > 0$, the
447 hypothesis dictates that C1 ought to be located on the dawn cell when above the neutral
448 sheet and the dusk cell when below, at least in the case that the spacecraft is close to
449 midnight (Grocott et al., 2007). This might be true statistically, but does not account for the
450 dusk-dawn location of the spacecraft, which in this case was $6 \lesssim Y_{\text{GSM}} \lesssim 7 R_E$. If, as a result,

451 the spacecraft was actually located on the dusk cell when above the neutral sheet, and on
452 the dawn cell when below the neutral sheet, then the sense of the observed plasma sheet
453 flows would actually be consistent with the large-scale convection.

454

455 One way to specify which cell the spacecraft is located within is to map its location into the
456 ionosphere. This has been done using TA15 and is shown by the crosses (X) on the northern
457 hemisphere convection maps and by plus signs (+) on the southern hemisphere convection
458 maps, in Fig. 4a and 4b, respectively. Firstly, let us consider the northern hemisphere map
459 from 00:24 – 00:26 UT in Fig. 4a: despite the lack of scatter in the immediate vicinity of the
460 spacecraft footprints, it is noticeable how the spacecraft appear to map closer to the dusk
461 cell than the dawn cell. For the remaining northern hemisphere maps, there is insufficient
462 scatter to determine the exact division between the dusk and dawn convection cells, such
463 that it is inconclusive as to which cell the Cluster spacecraft map to when above the neutral
464 sheet. If Cluster did indeed map to the dusk convection cell, then the duskward flows in the
465 northern hemisphere plasma sheet observed by C1 would actually be consistent with the
466 large-scale convection pattern. Furthermore, given that the C2-C4 magnetic field
467 observations are consistent with the local B_y being dominated by magnetotail flaring (as
468 opposed to IMF B_y) at the pre-midnight location of Cluster, it is likely that we would expect
469 the return sense of the convection to be dominated here by the symmetric (duskward)
470 element both above and below the neutral sheet (see e.g. Pitkänen et al., 2019).

471

472 If we instead consider the southern hemisphere maps in Fig. 4b we can be more certain of
473 which cell the spacecraft map to. Owing to the IMF B_y positive nature of the convection (i.e.
474 the more extended southern hemisphere dusk cell) and the pre-midnight location of the
475 spacecraft, the footprints are located quite convincingly on the dusk cell. This is despite the
476 dusk-dawn asymmetry being less pronounced than that seen in the northern hemisphere
477 (and the associated poorer coverage of southern hemisphere SuperDARN data). When
478 below the neutral sheet C1 observed dawnward flows, meaning it would have to have been
479 on the southern hemisphere dawn cell to be consistent with the large-scale convection,
480 which is clearly not the case. Indeed, the observed dawnward flow in the southern
481 hemisphere at this location could only be interpreted in terms of the untwisting hypothesis
482 for a situation where we had clear IMF $B_y < 0$ penetration (and associated extended dawn

483 cell), which has already been ruled out. C3, meanwhile, continually observed duskward flow,
484 which appears to be consistent with the larger-scale convection. It seems much more likely,
485 therefore, that C1 observed flow that was associated with localized magnetic field dynamics
486 rather than being a signature of the large-scale convection.

487

488

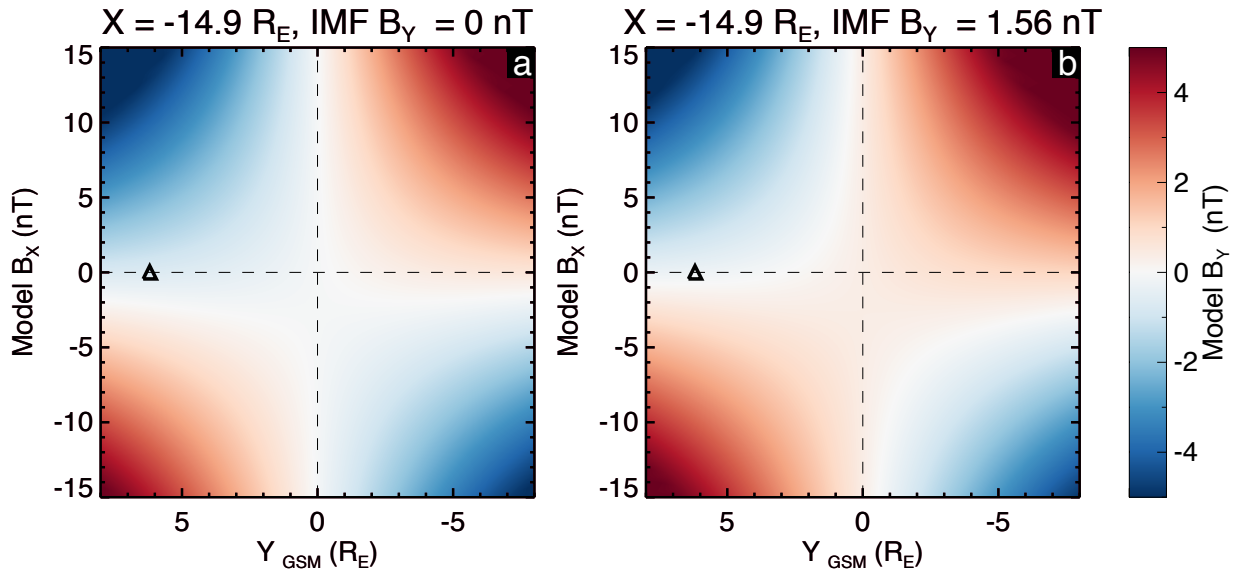
489 *4.2 Evidence for a local perturbation in the magnetotail*

490 The lack of consistency with the large-scale convection leads us to a third explanation for
491 our observations, which is that there is a local perturbation within the tail that is
492 independent of any large-scale, IMF B_y -controlled asymmetry associated with magnetotail
493 untwisting. This is supported by the observations from the other Cluster spacecraft. The
494 low-level of flow seen by C3 is mostly duskward (Fig. 3v), which would be consistent with
495 untwisting for IMF $B_y > 0$, given its southern hemisphere location. We note, however, that
496 due to the pre-midnight location of C3, one would also rightly expect to observe duskward
497 flow even in the case that there was no IMF $B_y > 0$ control (e.g. Kissinger et al., 2012) .
498 Further, in Fig. 2b v), up until the rapid B_x variations began at ~00:24 UT, fast duskward flow
499 in the southern hemisphere was also seen by C1. The fact that C3 continued to then observe
500 steady duskward flow, and no significant B_x change, suggests that the change in the nature
501 of the C1 observations after 00:24 UT must in-fact be due to some localized process that
502 was responsible for driving the dawnward component of the flows which was only observed
503 by C1.

504

505 This idea of a local perturbation is also supported by the variations in the local B_y
506 component. Fig. 3 ii) illustrates the in-situ variations in B_y with time across the interval.
507 Despite there clearly being positive IMF B_y penetration globally (as confirmed by inspection
508 of the OMNI and SuperDARN data), C1, C2 and C4 all recorded mostly negative local B_y
509 values. In the studies of, e.g., Pitkänen et al. (2013, 2017) this observation would have been
510 offered as evidence of a negative of IMF B_y penetration, thus supporting the untwisting
511 hypothesis. However, it is important to note that a negative local B_y component may be
512 wholly consistent with positive IMF B_y . There are, in fact, multiple sources of B_y in the tail,
513 such as magnetotail flaring (Fairfield, 1979), as well as tilt effects and current sheet warping
514 (see e.g. Petrukovich et al., 2005), in addition to a penetration of the IMF B_y . To fully

515 interpret the magnetic field observations, we must therefore consider the possible effects
 516 of these phenomena on the presence of B_y in the tail at the specific location of each
 517 spacecraft.



518
 519

520 **Figure 5:** TA15 model magnetic field data. In each case, plotted is Y vs B_x [GSM], (at
 521 $X = -14.9 R_E$, i.e. the X position of C1 at $\sim 00:28$ UT on 12 Oct 2006), with the TA15 modelled
 522 B_y value shown by the color bar on the right. The black triangle shows the Y -location of C1,
 523 at $B_x = 0$. In panel (a) we have imposed IMF $B_y = 0$, and for panel (b) we have used the 1-
 524 hour mean-averaged IMF B_y (+1.56 nT) in the hour prior to 00:28 UT.

525

526 To aid in this interpretation, we present TA15 model magnetic field data in Figure 5, to
 527 provide an indication of the expected background B_y -component at the time of our interval.
 528 These data, from $X = -14.9 R_E$, are plotted against Y [GSM]-position on the horizontal axis,
 529 and against the B_x -component on the vertical axis. We have reversed the conventional
 530 direction of the horizontal axis (negative to positive from left to right) to be consistent with
 531 a view looking earthward from downtail. In panel (a) we show the field for the case that IMF
 532 $B_y = 0$ and in panel (b) the case that IMF $B_y = +1.56$ nT (the 1-hour mean-averaged IMF B_y in
 533 the hour prior to 00:28 UT). The first conclusion we can make from consideration of the B_y
 534 component in Fig. 5a is how, even under no IMF B_y penetration, a ‘background’ B_y value will
 535 exist in the tail purely dependent on location. In such a ‘symmetric’ tail, one would expect
 536 the background B_y value to appear as one moves away from midnight toward the dusk-

537 dawn flanks, as well as further above and below the neutral sheet. Pre-midnight, we would
538 expect to observe negative B_y above the neutral sheet ($B_x > 0$), and positive B_y below the
539 neutral sheet ($B_x < 0$), with the opposite effect post-midnight. This is the well-known
540 magnetotail flaring effect (Fairfield, 1979).

541

542 The data in Fig. 5a also show the effect of the negative (tailward) dipole tilt (as appropriate
543 to our study interval) and current sheet warping on the local B_y component. According to
544 Petrukovich (2011), the current sheet warping (controlled by the dipole tilt) is expected to
545 add a negative B_y component pre-midnight and a positive B_y component post-midnight.
546 Furthermore, the ‘even tilt’ effect is expected to add a negative B_y component to both the
547 pre and post-midnight sectors for a negative tilt. This leads to the effect seen in Fig. 5a
548 where in the pre-midnight sector, the location of the B_y polarity change occurs in the
549 southern hemisphere (at $B_x \approx -3$ nT).

550

551 Fig. 5b illustrates the scenario relevant to our case study, where we have additionally a
552 global positive IMF B_y penetration. This additional positive B_y has the effect of moving the
553 location of the pre-midnight B_y polarity change back up towards the neutral sheet. This
554 explains why the Cluster spacecraft observed $B_y \approx 0$ at times of $B_x \approx 0$ during the few tens of
555 minutes prior to our interval, as noted in section 3.2. This also explains why C2-3 and C4
556 observed the polarity of B_y that they did throughout the interval. It is thus clear that positive
557 IMF B_y penetration does not mean we should expect to observe positive B_y everywhere in
558 the tail, rather, it simply means that there is expected to be some positive B_y perturbation
559 to the already present ‘background’ B_y at a particular location. As Fig. 5b demonstrates, C2
560 and C4 (located above the neutral sheet) are expected to have observed negative B_y even
561 though positive IMF B_y has penetrated into the magnetotail, illustrating that the flaring
562 effect is generally dominant at the spacecraft location. The background B_y expected at their
563 location (pre-midnight, $B_x > 0$), is negative and the IMF B_y -associated perturbation was not
564 large enough to enforce a sign change in B_y .

565

566 The Cluster spacecraft in our study were all located pre-midnight (+Y GSM). From Figure 3,
567 C2 and C4 observed positive B_x , and negative B_y , and at ~00:28 UT were located at around
568 $Z = -1 R_E$ (Figure 1). C3, however, observed negative B_x and positive B_y , and was located at

569 around $Z = -2.5 R_E$. The location of the neutral sheet at $\sim 00:28$ UT can therefore be said
570 (locally) to have been somewhere between -1 and $-2.5 R_E$ in Z . C1 was located at around $Z =$
571 $-1.5 R_E$ and, throughout the five-minute interval, observed a B_x which continually fluctuated
572 from positive to negative, yet observed mostly weakly negative B_y . For B_y to have remained
573 negative, despite C1 moving above and below the neutral sheet, suggests that there was a
574 B_y negative ‘kink’ in the magnetotail that was localized to the vicinity of C1. This is further
575 supported by the fact that numerous (albeit brief) positive B_y excursions occurred when C1
576 was above the neutral sheet (as noted in section 3.2). We use the term ‘kink’ to highlight a
577 deformation in the nearby field lines which results in the observed perturbations to the local
578 B_y component. We suggest that this deformation could be relatively small in terms of field
579 line length, much like a kink in a cable or wire. In the following section, we investigate this
580 kink in relation to the observed current sheet flapping.

581

582

583 *4.3 Evidence for current sheet flapping as a source of the asymmetric flows*

584 If a localized magnetic field perturbation was associated with the lack of observation of the
585 expected dusk-dawn flow for magnetotail untwisting, investigating its cause seems a
586 worthwhile endeavour. The clear sinusoidal-like variation in B_x observed by C1, which is
587 evidence of current sheet flapping (e.g. Runov et al., 2009), provides us with a starting point
588 for this investigation. This flapping must be either highly localized or low in amplitude, as at
589 the time of our five-minute flow interval (00:28 -00:33 UT), only C1 observed the flapping.
590 MVA analysis (Sonnerup & Cahill, 1967) suggests that the flapping was a kink-like wave
591 which was propagating dawnward (Rong et al., 2015; Wu et al., 2016), and therefore may
592 have been a source of the observed dusk-dawn flow.

593

594 The causes of current sheet flapping have been discussed previously (Runov et al., 2009;
595 Wei et al., 2019). One such cause has been attributed to localized, periodical reconnection –
596 a process known to drive Bursty Bulk Flows (BBFs) in the magnetotail (Angelopoulos et al.,
597 1994; Zhang et al., 2016). In fact, BBFs excited directly as a result of reconnection in the tail
598 have been previously linked to magnetic fluctuations in the current sheet (Nakamura et al.,
599 2009; Wu et al., 2016). Examining the data presented in Fig. 3 iii) and Fig. 3 iv), we note that
600 C1 measured a generally positive B_z , with a few negative blips, as well as continually fast (v_x

601 > 200 km s⁻¹) earthward flow, peaking at over 370 km s⁻¹ with bursts of enhanced
 602 convective flow ($v_{\perp x} > 200$ km s⁻¹) also apparent. These observations are fairly consistent
 603 with (if slightly slower than) the original definition of a BBF (Angelopoulos et al., 1994). This,
 604 along with the absence of similar flow observations in the C3 data, suggests that C1 may
 605 have been located earthward of a localized reconnection site (owing to $B_z > 0$), where
 606 persistent, localized reconnection was exciting fast earthward flow. The reconnection
 607 process may then have been driving the current sheet flapping, inducing the localized kink in
 608 the field, and ultimately controlling the dusk-dawn direction of the convective flow.

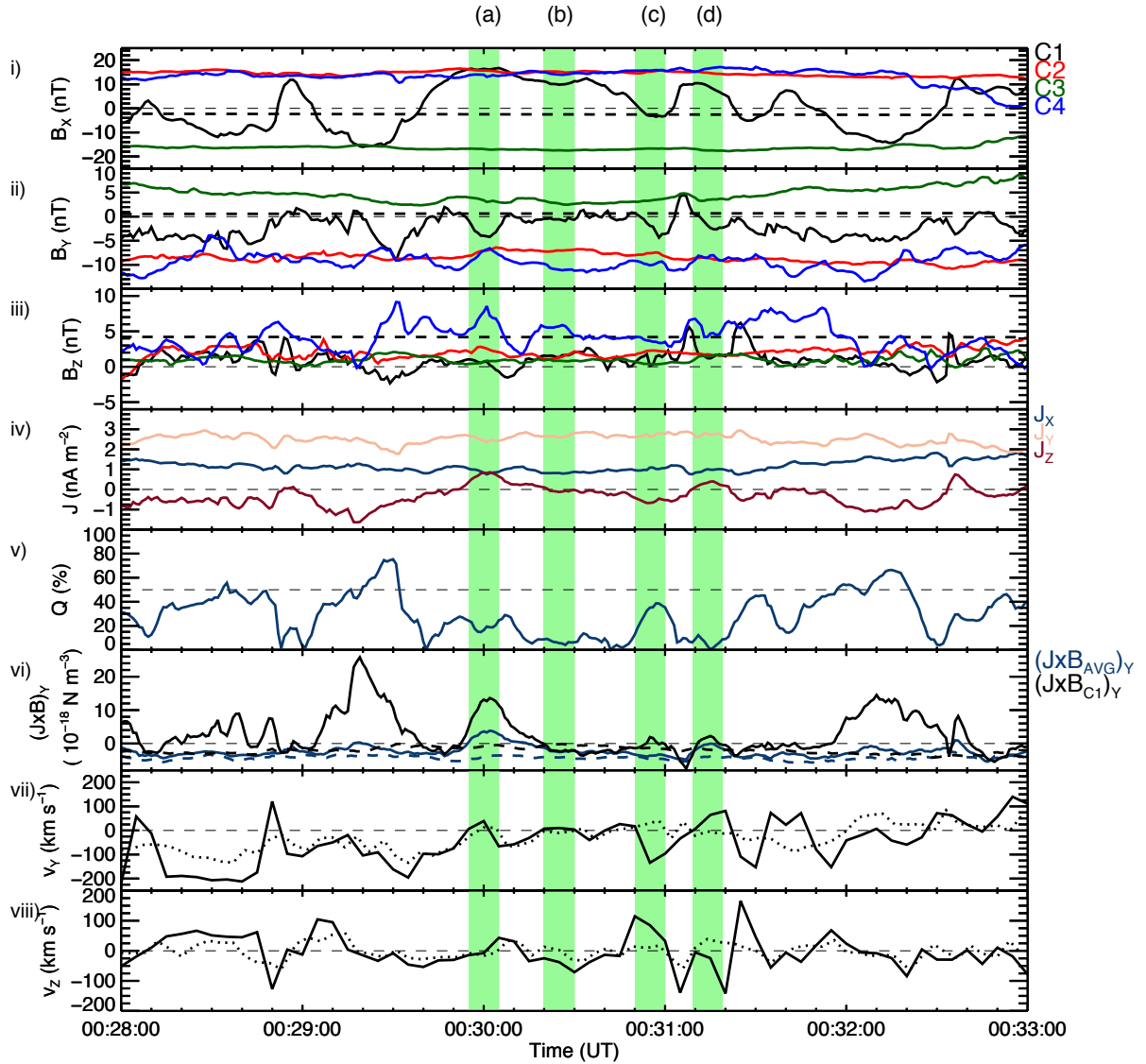
609

610

611 It is well known that the magnetic tension force is responsible for the acceleration of plasma
 612 following reconnection (Karlsson et al., 2015). Our observations of a dusk-dawn flow
 613 component may be related to the localized magnetic tension forces driving and directing
 614 plasma flows in association with the flapping. In order to provide some scope to this
 615 suggestion, we attempted to find the direction of the $\mathbf{J} \times \mathbf{B}$ forces acting on the plasma. We
 616 used the curlometer technique (Dunlop et al., 1988, 2002), to estimate the average current
 617 density, \mathbf{J} , flowing through the volume bound by the spacecraft tetrahedron. The $\mathbf{J} \times \mathbf{B}$
 618 force density [N m⁻³] is then calculated, firstly, by taking the cross product of \mathbf{J} with the
 619 average magnetic field vector \mathbf{B} from the four-spacecraft (\mathbf{B}_{AVG}). We also calculate $\mathbf{J} \times \mathbf{B}$
 620 using solely \mathbf{B} from C1 (\mathbf{B}_{C1}), in order to provide a more local estimate for $\mathbf{J} \times \mathbf{B}$ at the
 621 location of C1.

622

623 In order to check the validity of using the curlometer approach, we calculated the quality
 624 parameter, Q , defined as $|\nabla \cdot \mathbf{B}|/|\nabla \times \mathbf{B}|$. It is generally accepted that a value of $Q < 0.5$ is
 625 required for a current estimate to be valid. Hence, the value of Q , along with due
 626 consideration of the spacecraft configuration and its orientation relative to the magnetic
 627 field structure, may be used as a monitor of how reliable the curlometer approach is
 628 (Dunlop et al., 2002). This is discussed further below, in reference to the analysis shown in
 629 Figure 6.



630

631

632

633

634

635

636

637

638

639

640

641

Figure 6: i-iii) The local magnetic field vector \mathbf{B} (B_x , B_y , B_z) observed by C1-4, as shown previously (solid lines) and the TA15 modelled \mathbf{B} vector for C1 (dashed black lines). iv) The components of the current density vector \mathbf{J} (J_x , J_y , J_z), v) Q , vi) $(\mathbf{J} \times \mathbf{B}_{AVG})_y$ (solid blue line) and $(\mathbf{J} \times \mathbf{B}_{C1})_y$ (solid black line). The dashed blue and black lines indicate the equivalent calculation where the TA15 model \mathbf{B} field of C1 has been used (see text). vii) v_y ($v_{\perp y}$ in solid lines), observed by C1 and viii) v_z ($v_{\perp z}$ in solid lines), also observed by C1. The green highlighted regions labelled (a), (b), (c) and (d) correspond to four specific time-windows of interest (discussed in-text).

Shown in Fig. 6 i-iii) are the local magnetic field B_x , B_y and B_z components, as presented previously. In Fig. 6 iv) are the current density J_x , J_y and J_z components determined from the

642 curlometer analysis. In Fig. 6 vi) is the dusk-dawn component of $\mathbf{J} \times \mathbf{B}_{AVG}$ and $\mathbf{J} \times \mathbf{B}_{C1}$.
 643 Finally, in Fig. 6 vii) and viii) are the dusk-dawn and north-south components of the flow
 644 (and field-perpendicular flow) observed by C1, as shown previously. In panels (i-iii), the
 645 dashed black line represents the TA15 modelled magnetic field (see section 4.2) at the
 646 location of C1. In panel (vi) the dashed blue and black lines represent the $(\mathbf{J} \times \mathbf{B}_{AVG})_y$ and $(\mathbf{J}$
 647 $\times \mathbf{B}_{C1})_y$ forces, respectively, where \mathbf{J} and $\mathbf{J} \times \mathbf{B}$ have been computed using the model field
 648 at the location of C1 and the true magnetic fields measured by C2-C4. These ‘model $(\mathbf{J} \times \mathbf{B})_y$
 649 forces’ have been computed to provide an illustration of what one would expect the
 650 ‘unperturbed’ magnetic field of C1 and the associated $(\mathbf{J} \times \mathbf{B})_y$ force to look like, in the
 651 absence of any dynamical effects such as current sheet flapping or field line ‘kinking’. In
 652 both cases, the model $(\mathbf{J} \times \mathbf{B})_y$ forces are weakly downward, consistent with the
 653 ‘background curvature’ of the magnetic field at this pre-midnight location (see Fig. 7). Fig. 6
 654 v) suggests that our curlometer approach is generally appropriate, as Q mostly remains
 655 below 50% (horizontal dashed line) for the five-minute interval. We note that, unlike in
 656 previous studies which have used the curlometer technique at inter-spacecraft separation
 657 distances of $\ll 1 R_E$ (e.g. Dunlop et al., 2002; Runov et al., 2003), in our case the Cluster
 658 spacecraft separation is large ($\gtrsim 1 R_E$). Therefore, the curlometer is likely to be an
 659 underestimate of the true current at these scale sizes. Critically, however, the spacecraft
 660 configuration is such that the estimate of the direction of the currents should be stable.
 661 Thus, although the volume enclosed by the spacecraft is greater than the scale sizes of the
 662 current sheet flapping and kink, a reliable estimate of the direction of the net $\mathbf{J} \times \mathbf{B}$ force
 663 within the enclosed volume may still be obtained.

664
 665 Two key features of Figure 6 are apparent. Firstly, it appears as though the perturbations to
 666 $(\mathbf{J} \times \mathbf{B})_y$ are mostly associated with the magnetic field perturbations generally only observed
 667 by C1. This is made apparent by comparing $(\mathbf{J} \times \mathbf{B}_{C1})_y$ with $(\mathbf{J} \times \mathbf{B}_{AVG})_y$, where the
 668 perturbations are much larger in magnitude for $(\mathbf{J} \times \mathbf{B}_{C1})_y$. We also note that both
 669 $(\mathbf{J} \times \mathbf{B}_{AVG})_y$ and $(\mathbf{J} \times \mathbf{B}_{C1})_y$ are effectively always positive with respect to their model
 670 equivalents. However, $(\mathbf{J} \times \mathbf{B}_{AVG})_y$ is still mostly net negative whereas $(\mathbf{J} \times \mathbf{B}_{C1})_y$ is net
 671 positive. This suggests that using \mathbf{B}_{C1} , rather than \mathbf{B}_{AVG} in calculating $(\mathbf{J} \times \mathbf{B})_y$ has overall

672 reduced the effects of the larger-scale background field curvature (incorporated by
673 including the other spacecraft). Second, the magnetic field and flow dynamics evident in Fig.
674 6 appear to almost always be associated with positive (duskward) enhancements in $(\mathbf{J} \times \mathbf{B})_y$,
675 in contrast to the model dawnward sense of $(\mathbf{J} \times \mathbf{B})_y$. This is particularly evident in the case
676 of $(\mathbf{J} \times \mathbf{B}_{C1})_y$, but also generally true in the case of $(\mathbf{J} \times \mathbf{B}_{AVG})_y$. We therefore suggest that
677 the dynamic behaviour of $(\mathbf{J} \times \mathbf{B})_y$ is simply consistent with the localized kinks and flapping
678 in the magnetic field that are associated with the transient perturbations to the dusk-dawn
679 flow observed by C1.

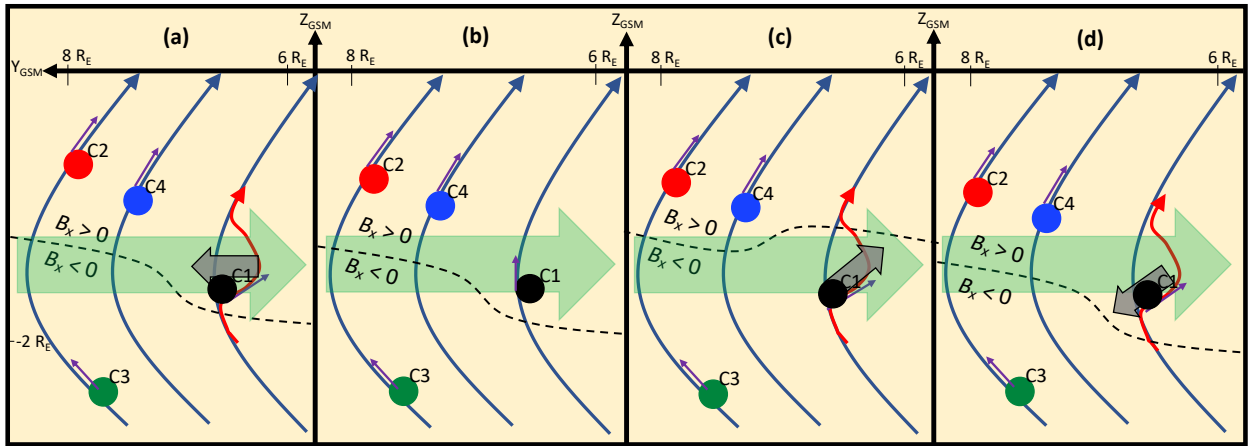
680

681

682 *4.4 Visualization of the observed dynamics*

683 In an effort to visualize these plasma sheet dynamics, we show in Figure 7 a series of
684 sketches that attempt to associate the observed magnetic field perturbations with the
685 observed dusk-dawn convective flows. The panels correspond to the four time-windows
686 indicated on Figure 6 by the highlighted regions labelled a-d. In each panel, we indicate the
687 approximate relative position of the 4 Cluster spacecraft in GSM coordinates, and the
688 appropriate sense of B_y measured by each spacecraft is shown by the purple arrows at each
689 spacecraft location (the Z-component of the field was in fact generally small, and has been
690 exaggerated here for illustrative purposes). We also superimpose nominal plasma sheet
691 field lines (again with an exaggerated extent in Z) that display the sense of B_y implied by the
692 TA15 data presented in Figure 5 (long blue curved arrows). The dashed lines represent the
693 location of the neutral sheet at the end of each time window. This is tilted slightly, as
694 appropriate for IMF $B_y > 0$, but with the end-state of the “flap” of the current sheet implied
695 by the sign of B_x observed by C1. In red is the perturbation to the field implied by the sign of
696 B_y observed by C1.

697



698

699

700 **Figure 7:** Schematic diagrams of the observed magnetic field perturbations and dusk-dawn

701 convective flows during the time-windows indicated in Fig. 6 by the highlighted regions. The

702 approximate locations of the four Cluster spacecraft relative to one-another in the Y-Z GSM

703 plane are indicated (not to scale) by the colored circles. The curved blue arrows represent

704 magnetic field lines, and the short purple arrow indicates the local sense of B_y at the

705 location of each spacecraft. The dashed black line indicates the current sheet. In panels (a),

706 (c) and (d), the curved red arrow shows the ‘kinked’ magnetic field line. The long thick green

707 arrow shows the direction of the model $(\mathbf{J} \times \mathbf{B})_y$ force associated with the background

708 curvature of the magnetic field, and the small thick gray arrow shows the direction of the

709 dusk-dawn convective flow observed by C1.

710

711

712 In Fig. 7a C1 is located above the current sheet and measured negative B_y . A weakly

713 duskward convective flow was observed at this time (as indicated by the thick gray arrow),

714 consistent with the duskward sense of the $(\mathbf{J} \times \mathbf{B})_y$ force, and opposite to the sense of the

715 model $(\mathbf{J} \times \mathbf{B})_y$ force associated with the background curvature of the magnetic field. In Fig.

716 7b, C1 is still above the current sheet but measured $B_y \approx 0$ and no dusk-dawn convective

717 flow. In Fig. 7c C1 is shown below the current sheet, where the background B_y would be

718 positive (see Fig. 5b). C1 instead observed an increasingly negative B_y , which we suggest is

719 associated with the presence of the kink in the field. At the same time, C1 also observed a

720 convective plasma flow with downward and slightly upward (+Z) component (thick gray

721 arrow). We therefore suggest that the flow was associated with the upward/dawnward flap
722 of the current sheet, and that the dawnward sense of the flow likely also resulted in the
723 increase in negative B_y seen during the time-window shown in Fig. 6c. The positive
724 $(\mathbf{J} \times \mathbf{B}_{C1})_y$ at this time, whilst inconsistent with the dawnward sense of the flow, is therefore
725 consistent with the curvature of the magnetic field associated with the kink. $(\mathbf{J} \times \mathbf{B}_{AVG})_y$,
726 meanwhile, was negative, likely due to incorporating the larger-scale background curvature
727 of the magnetic field observed by the other spacecraft. In Fig. 7d C1 is shown above the
728 current sheet, where it observed a weakly negative B_y . In this case, C1 observed a
729 convective plasma flow with duskward and slightly downward ($-Z$) component. Similarly to
730 in Fig. 7a, this flow occurred in concert with a positive enhancement in $(\mathbf{J} \times \mathbf{B})_y$ relative to
731 the model $(\mathbf{J} \times \mathbf{B})_y$. This flow would therefore seem to be associated with the downward
732 flap of the current sheet, and its duskward sense could indicate that it is acting to reduce
733 the negative kink in B_y that is apparent over the time-window shown in Fig. 6d.

734

735 Whilst we acknowledge a degree of uncertainty in the details of the interpretation
736 presented above of the specific relationship between the flows and the field, it serves to
737 illustrate three observations about this interval of which we can be very certain: 1) The IMF,
738 ionospheric convection, and comparison of the plasma sheet magnetic field observations to
739 the TA15 model field, all lead to the expectation of an IMF $B_y > 0$ large-scale asymmetry in
740 the magnetosphere. 2) The Cluster 1 spacecraft observed convective flow with a dusk-dawn
741 component that was inconsistent with current theories of IMF B_y -induced dusk-dawn flows
742 associated with magnetotail untwisting. Notably, the observed dawnward flow in the
743 southern hemisphere, whilst inconsistent with IMF $B_y > 0$, was also inconsistent with the
744 expected (symmetric) duskward flow at this pre-midnight location even in the absence of
745 IMF B_y control. 3) Magnetic field perturbations that were indicative of a localized current
746 sheet flapping and dusk-dawn kink in the field occurred coincident with the flows. It
747 therefore seems likely that in this case the IMF B_y -driven asymmetry, or indeed the
748 symmetric flow expected at the spacecraft location, was being overridden by the localized
749 dynamics in governing the dusk-dawn component of the flow.

750

751

752 **5. Summary**

753

754 We have presented a case study from 12 October 2006 revealing a dynamic interval of
755 plasma flows and current sheet flapping, observed by the Cluster 1 spacecraft. The key
756 observations presented in this study may be summarised as follows:

757

758 • The OMNI data revealed that the IMF B_y had been positive for several hours prior to
759 our interval of Cluster data, with the exception of three short-lived negative
760 excursions.

761 • The SuperDARN ionospheric convection observations revealed a large-scale
762 asymmetry consistent with IMF $B_y > 0$, confirming the absence of a large-scale
763 asymmetry in the flow pattern that might explain the dawnward flows observed by
764 C1.

765 • C1 observed a changing B_x magnetic field component and associated duskward ($v_{\perp y}$
766 > 0) flow when in the northern magnetic hemisphere, and dawnward ($v_{\perp y} < 0$) flow
767 in the southern magnetic hemisphere.

768 • The C2, C3 and C4 magnetic field observations suggested that the local B_y was being
769 dominated by magnetotail flaring, as opposed to IMF B_y . C3 also observed duskward
770 flow in the southern magnetic hemisphere, consistent with the symmetric flow
771 expected owing to the pre-midnight location of the spacecraft.

772

773 Contrary to the results of a number of previous studies in the literature, during this
774 particular interval, the dusk-dawn sense of the convective magnetotail flows ($v_{\perp y}$); and in
775 particular, the dawnward flow observed in the southern hemisphere, does not agree with
776 expectations based on the theoretical understanding of global magnetotail untwisting and
777 the prevailing positive IMF B_y conditions, nor to expectations based on the location of the
778 spacecraft and associated magnetotail flaring. We instead attribute the flows to a localized
779 magnetic field perturbation, or 'kink' in the magnetotail, which appears to have been
780 independent of any large-scale dynamics and may have instead been related to the
781 observed current sheet flapping. We attributed the current sheet flapping to being driven
782 by localized reconnection, itself inferred from the presence of the observed bursty fast

783 earthward flow ($v_{\perp x} \approx 200 \text{ km s}^{-1}$). Analysis using the curlometer technique suggests that
 784 the $(\mathbf{J} \times \mathbf{B})_y$ force is consistent with the localized kinks and flapping in the magnetic field
 785 that are associated with the transient perturbations to the dusk-dawn flow observed by C1.

786

787

788 Although evidence for the large-scale penetration of IMF $B_y > 0$ is apparent, the IMF $B_y > 0$
 789 penetration at the location of C1 appears to have been unable to override the variable dusk-
 790 dawn flow associated with the current sheet flapping. Further studies by the authors are
 791 currently underway to determine if such flows are a frequent occurrence, and to consider,
 792 and account for, localized tail dynamics more fully in a statistical analysis of the magnetotail
 793 flows.

794

795 **Acknowledgements**

796

797 The authors would like to thank the FGM and CIS teams as part of the Cluster mission and
 798 acknowledge the Cluster Science Archive (Laakso et al., 2010) as the source of the Cluster
 799 data. We also wish to thank the OMNIWeb as the source of the solar wind and IMF data.
 800 The authors acknowledge the use of SuperDARN data. SuperDARN is a collection of radars
 801 funded by national scientific funding agencies of Australia, Canada, China, France, Italy,
 802 Japan, Norway, South Africa, United Kingdom, and United States of America, and we thank
 803 the international PI team for providing the data. The authors acknowledge access to the
 804 SuperDARN database via BAS data mirror (<http://bslsuperdarn.nc.nerc-bas.ac.uk:8093/docs/>)
 805 and are grateful for use of the Radar Software Toolkit (RST v4.2
 806 <https://zenodo.org/record/1403226#.Xy0u7y3MxTY>) with which the raw radar data were
 807 processed. We acknowledge the WDC for Geomagnetism, Kyoto, for use of the auroral
 808 electrojet indices, which may be obtained from <http://wdc.kugi.kyoto-u.ac.jp/aedir/>. We are
 809 also grateful to Haje Korth for providing the IDL Geopack DLM containing the Tsyganenko
 810 magnetic field model routines and coordinate system conversions and wish to thank Nikolai
 811 Tsyganenko for useful discussion of his magnetic field models. Finally, we are thankful for
 812 the advice of Malcolm Dunlop regarding the applicability of the curlometer technique at
 813 large spacecraft separations. This research was undertaken with the support of funding
 814 from the following sources: Lancaster University Faculty of Science and Technology
 815 studentship (JHL), STFC Consolidated grant no. ST/R000816/1 (NAC, AG), NERC standard
 816 grant nos. NE/P001556/1 and NE/T000937/1 (MTW, AG).

817

818 **References**

819

820 Angelopoulos, V., Baumjohann, W., Kennel, C. F., Coroniti, F. V., Kivelson, M. G., Pellat, R.,
 821 Walker, R. J., Lühr, H. and Paschmann, G. (1992). Bursty bulk flows in the inner central
 822 plasma sheet. *J. Geophys. Res.*, 97 (A4), 4027-4039. doi:10.1029/91JA02701

823

- 824 Angelopoulos, V., Kennel, C. F., Coroniti, F. V., Pellat, R., Kivelson, M. G., Walker, R. J.,
825 Russell, C. T., Baumjohann, W., Feldman W. C. and Gosling, J. T. (1994). Statistical
826 characteristics of bursty bulk flow events. *J. Geophys. Res.*, *99 (A11)*, 21,257-21,280.
827 doi:10.1029/94JA01263
828
- 829 Balogh, A., Carr, C. M., Acuña, M. H., Dunlop, M. W., Beek, T. J., Brown, P., Fornacon, K. -H.,
830 Georgescu, E., Glassmeier, K. -H., Harris, J., Musmann, G., Oddy, T. and Scwingenschuh, K.
831 (2001). The Cluster magnetic field investigation: Overview of in-flight performance and
832 initial results. *Ann. Geophys.*, *19*, 1207-1217. doi: 10.5194/angeo-19-1207-2001
833
- 834 Baumjohann, W., Paschmann, G. and Cattell, C. A. (1989). Average Properties in the Central
835 Plasma Sheet. *Journal of Geophysical Research*, *94 (A6)*, 6597-6606. doi:
836 10.1029/JA094iA06p06597
837
- 838 Browett, S. D., Fear, R. C., Grocott, A., and Milan, S. E. (2017). Timescales for the penetration
839 of IMF B_y into the Earth's magnetotail. *J. Geophys. Res.: Space Physics*, *122 (1)*, 579-593.
840 doi:10.1002/2016JA023198
841
- 842 Cao, J. B., Ma, Y. D., Parks, G., Rème, H., Dandouras, I., Nakamura, R., Zhang, T. L., Zong, Q.,
843 Lucek, E., Carr, C. M., Liu, Z. X. and Zhou, G. C. (2006). Joint observations by Cluster satellites
844 of bursty bulk flows in the magnetotail. *J. Geophys. Res.*, *111 (A4)*, A04206.
845 doi:10.1029/2005JA011322
846
- 847 Case, N. A., Grocott, A., Haaland, S., Martin, C. J., and Nagai, T. (2018). Response of the
848 Earth's Neutral Sheet to Reversals in the IMF B_y component. *J. Geophys. Res.*, *123 (10)*,
849 8206-8218. doi:10.1029/2018JA025712
850
- 851 Case, N. A. and Wild, J. (2012). A statistical comparison of solar wind propagation delays
852 derived from multispacecraft techniques. *J. Geophys Res.*, *117 (A2)*, A02101,
853 doi:10.1029/2011JA016946.
854
- 855 Chisham G., Lester, M., Milan, S. E., Freeman, M. P., Bristow, W. A., Grocott A., McWilliams,
856 K. A., Ruohoniemi, J. M., Yeoman, T. K., Dyson, P. L., Greenwald, R. A., Kikuchi, T., Pinnock,
857 M., Rash, J. P. S., Sato, N., Sofko, G. J., Villain, J. -P. and Walker, A. D. M. et al. (2007). A
858 decade of the Super Dual Auroral Radar Network (SuperDARN): scientific achievements,
859 new techniques and future directions. *Surveys in Geophysics* *28*, 33-109.
860 doi:10.1007/s10712-007-9017-8
861
- 862 Cowley, S. W. H. (1981). Magnetospheric asymmetries associated with the y-component of
863 the IMF. *Planet Space Sci*, *29 (1)*, 79-96. doi:10.1016/0032-0633(81)90141-0
864
- 865 Dungey, J. W. (1961). Interplanetary magnetic field and the auroral zones. *Phys. Rev. Lett.*, *6*,
866 47-48. doi:10.1103/PhysRevLett.6.47
867
- 868 Dunlop, M. W., Southwood, D. J., Glassmeier, K. -H., and Neubauer, F. M. (1988). Analysis of
869 multipoint magnetometer data. *Advances in Space Research*, *8 (9-10)*, 273-277.
870 doi:10.1016/0273-1177(88)90141-X

- 871
872 Dunlop, M. W., Balogh, A., Glassmeier, K. -H. and Robert, P. (2002). Four-point Cluster
873 application of magnetic field analysis tools: The Curlometer. *J. Geophys. Res.*, *107* (A11).
874 doi:10.1029/2001JA005088
875
876 Escoubet, C. P., Fehringer, M. and Goldstein, M. (2001). The Cluster Mission. *Ann. Geophys.*,
877 *19*, 1197 – 1200. doi:10.5194/angeo-19-1197-2001
878
879 Fairfield, D. H. (1979). On the Average Configuration Of The Geomagnetic Tail. *J. Geophys.*
880 *Res.*, *84* (A5), 1950-1958. doi:10.1029/JA084iA05p01950
881
882 Frühauff, D. and Glassmeier, K.-H. (2016). Statistical analysis of magnetotail fast flows and
883 related magnetic disturbances. *Ann. Geophys.*, *34*, 399-409. doi:10.5194/angeo-34-399-
884 2016
885
886 Grocott, A. (2017). Time Dependence of Dawn-Dusk Asymmetries in the Terrestrial
887 Ionospheric Convection Pattern. In: Haaland, S. et al. (2017), *Dawn-Dusk Asymmetries in*
888 *Planetary Plasma Environments*, John Wiley and Sons, Inc., 107-123
889
890 Grocott, A., Yeoman, T. K., Nakamura, R., Cowley, S. W. H, Frey, H. U., Rème, H. and Klecker,
891 B. J. (2004a). Multi-instrument observations of the ionospheric counterpart of a bursty bulk
892 flow in the near-Earth plasma sheet. *Ann. Geophys.*, *22*, 1061-1075, 1432-0576/ag/2004-22-
893 1061.
894
895 Grocott, A., Yeoman, T. K., Cowley, S. W. H, and Rème, H. (2004b). Multi-instrument
896 observations of bursty bulk flows and their ionospheric counterparts. *Proc. Seventh Internat.*
897 *Conf. on Substorms*, UDK-52-854, FMI, Helsinki, Finland, 107-110.
898
899 Grocott, A., Badman, S. V., Cowley, S. W. H, and Cripps (2004c). The influence of the IMF B_y
900 on the nature of the nightside high-latitude ionospheric flow during intervals of positive IMF
901 B_z . *Ann. Geophys.*, *22*, 1755-1764, doi:10.5194/angeo-22-1755-2004.
902
903 Grocott, A., Yeoman, T. K., Milan, S. E. and Cowley, S. W. H. (2005), Interhemispheric
904 observations of the ionospheric signature of tail reconnection during IMF-northward non-
905 substorm intervals, *Ann. Geophys.*, *23*, 1763–1770. doi:10.5194/angeo-23-1763-2005.
906
907 Grocott, A., Yeoman, T. K., Milan, S. E., Amm. O., Frey, H. U., Juusola, L., Nakamura, R.,
908 Owen, C. J., Rème, H. and Takada, T. (2007). Multi-scale observations of magnetotail flux
909 transport during IMF-northward non-substorm intervals. *Ann. Geophys.*, *25*, 1709-1720.
910 doi:10.5194/angeo-25-1709-2007
911
912 Grocott, A., Milan, S. E. and Yeoman, T. K. (2008). Interplanetary magnetic field control of
913 fast azimuthal flows in the nightside high-latitude ionosphere, *Geophys. Res. Lett.*, *35*,
914 L08102, doi:10.1029/2008GL033545.
915

- 916 Haaland, S., Runov, A. and Forsyth, C. (2017). Dawn-Dusk Asymmetries in Planetary Plasma
917 Environments, *Geophysical Monograph 230, First Edition. American Geophysical Union.*
918 Published 2017 by John Wiley & Sons, Inc.
919
- 920 Karlsson, T., Hamrin, M., Nilsson, H., Kullen, A., and Pitkänen, T. (2015). Magnetic forces
921 associated with bursty bulk flows in the Earth's magnetotail. *Geophys. Res. Lett.*, *42* (9),
922 3122-3128. doi:10.1002/2015GL063999
923
- 924 Kiehas, S. A., Runov, A., Angelopoulos, V., Hietala, H. and Korovinskiy, D. (2018). Magnetotail
925 Fast Flow Occurrence Rate and Dawn-Dusk Asymmetry at $X_{GSM} \sim -60 R_E$. *J. Geophys. Res.:
926 Space Physics*, *123* (3), 1767 – 1778. doi:10.1002/2017JA024776
927
- 928 King, J. H., and Papitashvili, N. E. (2005). Solar wind spatial scales in and comparisons of
929 hourly Wind and ACE plasma and magnetic field data. *J. Geophys. Res.*, *110*, A02104.
930 doi:10.1029/2004JA010649
931
- 932 Kissinger, J., McPherron, R. L., Hsu, T. -S. and Angelopoulos, V. (2012). Diversion of plasma
933 due to high pressure in the inner magnetosphere during steady magnetospheric convection.
934 *J. Geophys. Res.*, *117*, A05206. doi:10.1029/2012JA017579
935
- 936 Khurana, K. K., Walker, R. J., and Ogino, T. (1996). Magnetospheric convection in the
937 presence of interplanetary magnetic field By: A conceptual model and simulations. *J.
938 Geophys. Res.*, *101* (A3), 4907–4916. doi:10.1029/95JA03673
939
- 940 Kubyshkina, D. I., Sormakov, D. A., Sergeev, V. A., Semenov, V. S., Erkaev, N. V., Kubyshkin, I.
941 V., Ganushkina, N. Yu. And Dubyagin, S. V. (2014). How to distinguish between kink and
942 sausage modes in flapping oscillations? *J. Geophys. Res.*, *119*, 3,002-3,015.
943 doi:10.1002/2013JA019477.
944
- 945 Laakso, H., C. Perry, S. McCaffrey, D. Herment, A.J. Allen, C.C. Harvey, C.P. Escoubet, C.
946 Gruenberger, M.G.G.T. Taylor, and R. Turner (2010), Cluster Active Archive: Overview, 3-37,
947 The Cluster Active Archive, Astrophysics and Space Science Proceedings, H. Laakso et al.
948 (eds.), Springer.
949
- 950 Lockwood, M. (1993), Modelling high-latitude ionosphere for time-varying plasma
951 convection. IEE Proceedings-H, Vol. 140. No. 2. doi:10.1049/ip-h-2.1993.0015
952
- 953 Malova, H. V., Zelenyi, L. M., Popov, V. Y., Petrukovich, A. A. and Runov, A. V. (2007).
954 Asymmetric thin current sheets in the Earth's magnetotail. *Geophys. Res. Lett.*, *34* (16),
955 L16108. doi:10.1029/2007GL030011
956
- 957 McPherron, R. L., Hsu, T. -S., Kissinger, J., Chu, X., and Angelopoulos, V., (2011).
958 Characteristics of plasma flows at the inner edge of the plasma sheet. *J. Geophys. Res.*, *116*
959 (A5), A00133. doi:10.1029/2010JA015923
960
- 961 Nakamura, R., Baumjohann, W., Klecker, B., Bogdanova, Y., Balogh, A., Rème, H., Bosqued, J.
962 M., Dandouras, I., Sauvaud, J. A., Glassmeier, K. -H., Kistler, L., Mouikis, C., Zhang, T. L.,

- 963 Eichelberger, H. and Runov, A. (2002). Motion of the dipolarization front during a flow burst
964 event observed by Cluster. *Geophys. Res. Lett.*, *29* (20), 1942. doi:/10.1029/2002GL015763
965
- 966 Nakamura, R., Retinò, A., Baumjohann, W., Volwerk, M., Erkaev, N., Klecker, B., Lucek, E. A.,
967 Dandouras, I., André, M. and Khotyainstev, Y. (2009). Evolution of dipolarization in the near-
968 Earth current sheet induced by Earthward rapid flux transport. *Ann. Geophys.*, *27*, 1743-
969 1754. doi:10.5194/angeo-27-1743-2009
970
- 971 Ness, N. F. (1965). The Earth's Magnetic Tail. *J. Geophys. Res.*, *70* (13), 2989–3005.
972 doi:10.1029/JZ070i013p02989
973
- 974 Newell, P. T., Sotirelis, T., Liou, K., Meng, C. -I. and Rich, F. J. (2007). A nearly universal solar
975 wind-magnetosphere coupling function inferred from 10 magnetospheric state variables. *J.*
976 *Geophys. Res.*, *112* (A1), A01206. doi: 10.1029/2006JA012025
977
- 978 Nishitani, N., Ruohoniemi, J. M., Lester, M., Baker, J. B. H., Koustov, A. V., Shepherd, S. G.,
979 Chisham, G., Hori, T., Thomas, E. G., Makarevich, R. A., Marchaudon, A., Ponomarenko, P.,
980 Wild, J. A., Milan, S. E., Bristow, W. A., Devlin, J., Miller, E., Greenwald, R. A., Ogawa, T. and
981 Kikiuchi, T. (2019). Review of the accomplishments of mid-latitude Super Dual Auroral Radar
982 Network (SuperDARN) HF radars. *Progress in Earth and Planetary Science*, *6*:27.
983 doi:10.1186/s40645-019-0270-5
984
- 985 Ohma, A., Østgaard, N., Reistad, J. P., Tenfjord, P., Laundal, K. M., Moretto Jørgensen, T.,
986 Haaland, S. E., Krcelic, P. and Milan, S. (2019). Observations of Asymmetric Lobe Convection
987 for Weak and Strong Tail Activity. *J. Geophys. Res.: Space Physics*, *124* (12).
988 doi:10.1029/2019JA026773
989
- 990 Pettigrew, E. D., Shepherd, S. G. and Ruohoniemi, J. M. (2010). Climatological patterns of
991 high-latitude convection in the Northern and Southern hemispheres: Dipole tilt
992 dependencies and interhemispheric comparisons. *J. Geophys. Res.*, *115*, doi:
993 10.1029/2009JA014956.
994
- 995 Petrukovich, A. A. (2011). Origins of plasma sheet B_y . *J. Geophys. Res.*, *116* (A7), A07217.
996 doi:10.1029/2010JA016386
997
- 998 Petrukovich, A. A., Baumjohann, W., Nakamura, R., Schödel, R., and Mukai, T. (2001). Are
999 earthward bursty bulk flows convective or field-aligned? *J. Geophys. Res.*, *106* (A10), 21,211-
1000 21,215. doi:10.1029/2001JA900019
1001
- 1002 Petrukovich, A. A., Baumjohann, W., Nakamura, R., Runov, A., and Balogh, A. (2005). Cluster
1003 vision of the magnetotail current sheet on a macroscale. *J. Geophys. Res.*, *110* (A6), A06204.
1004 doi:10.1029/2004JA010825
1005
- 1006 Pitkänen, T., Hamrin, M., Norqvist, P., Karlsson, T., and Nilsson, H. (2013). IMF dependence
1007 of the azimuthal direction of earthward magnetotail fast flows. *Geophys. Res. Lett.*, *40* (21),
1008 5598-5604. doi:10.1002/2013GL058136
1009

- 1010 Pitkänen, T., Hamrin, M., Norqvist, P., Karlsson, T., Nilsson, H., Kullen, A., Imber, S. M. and
 1011 Milan, S. E. (2015). Azimuthal velocity shear within an earthward fast flow: further evidence
 1012 for magnetotail untwisting? *Ann. Geophys.*, *33*, 245-255. doi:10.5194/angeo-33-245-2015
 1013
- 1014 Pitkänen, T., Hamrin, M., Karlsson, T., Nilsson, H., and Kullen, A. (2017). On IMF B_y -Induced
 1015 Dawn-Dusk Asymmetries in Earthward Convective Fast Flows. In: Haaland, S. et al. (2017),
 1016 *Dawn-Dusk Asymmetries in Planetary Plasma Environments*, John Wiley and Sons, Inc., 107-
 1017 123.
 1018
- 1019 Pitkänen, T., Kullen, A., Laundal, K. M., Tenfjord, P., Shi, Q. Q. Park. J. -S., Hamrin, M., De
 1020 Spiegeleer, A., Chong, G. S. and Tian, A. M. (2019). IMF B_y Influence on Magnetospheric
 1021 Convection in Earth's Magnetotail Plasma Sheet. *Geophys. Res. Lett.*, *46* (21), 11,698-11,708.
 1022 doi:10.1029/2019GL084190
 1023
- 1024 Reistad, J. P., Østgaard, N., Tenfjord, P., Laundal, K. M., Snekvik, K., Haaland, S., Milan, S. E.,
 1025 Oksavik, K., Frey, H. U. and Grocott, A. (2016). Dynamic effects of restoring footprint
 1026 symmetry on closed magnetic field lines. *J. Geophys. Res.: Space Physics*, *121* (5),
 1027 015JA022058. doi:10.1002/2015JA022058
 1028
- 1029 Reistad, J. P., Østgaard, N., Laundal, K. M., Ohma, A., Snekvik, K., Tenfjord, P., Grocott, A.,
 1030 Oksavik, K., Milan, S. E. and Haaland, S. (2018). Observations of asymmetries in ionospheric
 1031 return flow during different levels of geomagnetic activity, *J. Geophys. Res.*, *123*.
 1032 doi:10.1029/2017JA025051
 1033
- 1034 Rème, H., Bosqued, J. M., Sauvaud, J. A., Cros, A., Dandouras, J., Aoustin, C., Bouyssou, J.,
 1035 Camus, Th., Cuvilo, J., Martz, C., Médale, J. L., Perrier, H., Romefort, D., Rouzaud, J., d'Uston,
 1036 C., Möbius, E., Crocker, K., Granoff, M., Kistler, L. M., Popecki, M., Hovestadt, D., Klecker, B.,
 1037 Paschmann, G., Scholer, M., Carlson, C. W., Curtis, D. W., Lin, R. P., McFadden, J. P.,
 1038 Formisano, V., Amata, E., Bavassano-Cattaneo, M. B., Baldetti, P., Belluci, G., Bruno, R.,
 1039 Chionchio, G., Di Lellis, A., Shelley, E. G., Ghielmetti, A. G., Lennartsson, W., Korth, A.,
 1040 Rosenbauer, H., Lundin, R., Olsen, S., Parks, G. K., McCarthy, M. and Balsiger, H. (1997). The
 1041 Cluster Ion Spectrometry (CIS) Experiment. *Space Sci. Rev.*, *79*, 303-350. doi:10.1007/978-
 1042 94-011-5666-0_12
 1043
- 1044 Rong, Z. J., Barabash, S., Stenberg, G., Futaana, Y., Zhang, T. L., Wan, W. X., Wei, Y. and
 1045 Wang, X. -D. (2015). Technique for diagnosing the flapping motion of magnetotail current
 1046 sheets based on single-point magnetic field analysis. *J. Geophys. Res.: Space Physics*, *120* (5),
 1047 3462-3474. doi:10.1002/2014JA020973
 1048
- 1049 Runov, A., Nakamura, R., Baumjohann, W., Zhang, T. L., Volwerk, M., Eichelberger, H. -U. and
 1050 Balogh, A. (2003). Cluster observations of a bifurcated current sheet. *Geophys. Res. Lett.*, *30*
 1051 (2), 1036. doi:10.1029/2002GL016136
 1052
- 1053 Runov, A., Angelopoulos, V., Sergeev, V. A., Glassmeier, K. -H., Auster, U., McFadden, J.,
 1054 Larson, D. and Mann, I. (2009). Global properties of magnetotail current sheet flapping:
 1055 THEMIS perspectives. *Ann. Geophys.*, *27*, 319-328. doi:10.5194/angeo-27-319-2009
 1056

- 1057 Ruohoniemi, J. M. and Baker, K. B. (1998). Large-scale imaging of high-latitude convection
1058 with Super Dual Auroral Radar Network HF radar observations. *J. Geophys. Res.*, *103* (A9),
1059 20,797-20,811. doi:10.1029/98JA01288
1060
- 1061 Ruohoniemi, J. M. and Greenwald, R. A. (1996). Statistical patterns of high-latitude
1062 convection obtained from Goose Bay HF radar observations. *J. Geophys. Res.*, *101* (A10),
1063 21,743-21,763. doi:10.1029/96JA01584
1064
- 1065 Sergeev, V. A., Angelopoulos, V., Gosling, J. T., Cattell, C. A., and Russell, C. T. (1996).
1066 Detection of localized, plasma-depleted flux tubes or bubbles in the midtail plasma sheet. *J.*
1067 *Geophys. Res.*, *101* (A5), 10,817 – 10,826. doi:10.1029/96JA00460
1068
- 1069 Sonnerup, B. U. Ö, and Cahill Jr, L. J. (1967). Magnetopause structure and attitude from
1070 Explorer 12 observations. *J. Geophys. Res.*, *72* (1), 171-183.
1071 doi:10.1029/JZ072i001p00171
1072
- 1073 Sonnerup, B. U. Ö and Scheible, M. (1998). Minimum and Maximum Variance Analysis. In:
1074 Paschmann, G. and Daly, W. (1998), *Analysis Methods for Multi-Spacecraft Data*, pp 185-
1075 220, ESA Publications Division, Noordwijk, Netherlands.
1076
- 1077 Tenfjord, P., Østgaard, N., Snekvik, K., Laundal, K. M., Reistad, J. P., Haaland, S., and Milan, S.
1078 E. (2015). How the IMF B_y induces a B_y component in the closed magnetosphere and how it
1079 leads to asymmetric currents and convection patterns in the two hemispheres. *J. Geophys.*
1080 *Res.: Space Physics*, *120* (11), 9368-9384. doi:10.1002/2015JA021579
1081
- 1082 Tenfjord, P., Østgaard, N., Strangeway, R., Haaland, S., Snekvik, K., Laundal, K. M., Reistad, J.
1083 P. and Milan, S. E. (2017). Magnetospheric response and reconfiguration times following
1084 IMF B_y reversals. *J. Geophys. Res.: Space Physics*, *122* (1), 417-431.
1085 doi:10.1002/2016JA023018
1086
- 1087 Thomas, E. G. and Shepherd, S. G. (2018). Statistical Patterns of Ionospheric Convection
1088 Derived From Mid-Latitude, High-Latitude and Polar SuperDARN HF Observations. *J.*
1089 *Geophys. Res.: Space Physics*, *123* (4), 3196-3216. doi:10.1002/2018JA025280
1090
- 1091 Tsyganenko, N. A. and Andreeva, V. A. (2015). A forecasting model of the magnetosphere
1092 driven by an optimal solar wind coupling function. *J. Geophys. Res.*, *120* (10), 8401-8425.
1093 doi:10.1002/2015JA021641
1094
- 1095 Volwerk, M., Zhang, T. L., Glassmeier, K. -H., Runov, A., Baumjohann, W., Balogh, A., Rème,
1096 H., Klecker, B. and Carr, C. (2008). Study of waves in the magnetotail region with cluster and
1097 DSP. *Advances in Space Research*, *41* (10), 1593-1597. doi:10.1016/j.asr.2007.04.005.
1098
- 1099 Wei, X. H., Cai, C. L., Cao, J. B., Rème, H., Dandouras, I., and Parks, G. K. (2015). Flapping
1100 motions of the magnetotail current sheet excited by nonadiabatic ions. *Geophys. Res. Lett.*,
1101 *42*, 4731-4735. doi:10.1002/2015GL064459
1102

- 1103 Wei, Y. Y., Huang, S. Y., Rong, Z. J., Yuan, Z. G., Jiang, K., Deng, X. H., Zhou, M., Fu, H. S., Yu,
1104 X. D., Xu, S. B., He, L. H. and Deng, D. (2019). Observations of Short-period Current Sheet
1105 Flapping Events in the Earth's Magnetotail. *The Astrophysical Journal Letters*, 874, 7pp.
1106 doi:10.3847/2041-8213/ab0f28/pdf.
1107
1108 Wu, M., Lu, Q., Volwerk, M., Vörös, Z., Ma, X., and Wang, S. (2016). Current sheet flapping
1109 motions in the tailward flow of magnetic reconnection. *J. Geophys. Res.*, 121 (8), 7817-7827.
1110 doi:10.1002/2016JA022819
1111
1112 Zhang, L. Q., Baumjohann, W., Wang, C., Dai, L., and Tang, B. B. (2016). Bursty bulk flows at
1113 different magnetospheric activity levels: Dependence of IMF conditions. *J. Geophys. Res.*,
1114 121 (9), 8773-8789. doi:10.1002/2016JA022397
1115
1116